nature biotechnology

Allele-specific silencing of mutant huntingtin and ataxin-3 genes by targeting expanded CAG repeats in mRNAs

Jiaxin Hu[1,4], Masayuki Matsui[1,4], Keith T Gagnon[1], Jacob C Schwartz[1], Sylvie Gabillet[3], Khalil Arar[3], Jun Wu[2], Ilya Bezprozvanny[2] & David R Corey[1]

Expanded trinucleotide repeats[1] cause many neurological diseases. These include Machado-Joseph disease (MJD)[2] and Huntington's disease (HD)[3], which are caused by expanded CAG repeats within an allele of the ataxin-3 (*ATXN3*) and huntingtin (*HTT*) genes, respectively. Silencing expression of these genes is a promising therapeutic strategy, but indiscriminate inhibition of both the mutant and wild-type alleles may lead to toxicity, and allele-specific approaches have required polymorphisms that differ among individuals. We report that peptide nucleic acid and locked nucleic acid antisense oligomers that target CAG repeats can preferentially inhibit mutant ataxin-3 and HTT protein expression in cultured cells. Duplex RNAs were less selective than single-stranded oligomers. The activity of the peptide nucleic acids does not involve inhibition of transcription, and differences in mRNA secondary structure or the number of oligomer binding sites may be important. Antisense oligomers that discriminate between wild-type and mutant genes on the basis of repeat length may offer new options for developing treatments for MJD, HD and related hereditary diseases.

Expanded trinucleotide repeats have been implicated in at least 19 inherited diseases[1], including MJD[2] and HD[3]. These diseases are autosomal dominant disorders with most patients expressing both mutant and wild-type alleles. Toxicity of the mutant protein is usually attributed to aggregation of the mutant protein or alteration of native protein-protein interactions. MJD, one of the most common ataxias with an incidence as high as 1 in 4,000 in some ethnicities [2], remains incurable. It is usually first diagnosed in adults, with patients eventually becoming wheelchair bound or bedridden, and is caused by expanded CAG repeats (12–39 repeats are normal, >45 repeats indicates disease) within the *ATXN3* gene. HD has an incidence of 5–10 per 100,000 individuals in Europe and North America[3,4]. Unaffected individuals have up to 35 repeats, whereas HD patients can have from 36 to >100 repeats[5]. The disease is characterized by adult onset and progressive neurodegeneration. Like MJD, there is no cure. HD is caused by the expansion of CAG trinucleotide repeats within the first exon of the *HTT* gene, leading to disruption of protein function and neurodegeneration.

Antisense oligonucleotides[6] or double-stranded RNAs[7–16] have been proposed as a therapeutic alternative to small-molecule drugs, which cannot disrupt the many toxic interactions formed between proteins and mutant HTT or ataxin-3 (ref. 17). Although small interfering (si)RNAs can inhibit HTT expression after infusion into the central nervous system[10], most double-stranded or antisense oligonucleotides tested to date inhibit expression of the mutant and wild-type protein indiscriminately[6–10]. HTT is known to play an essential role in embryogenesis, neurogenesis and normal adult function[18,19], raising concerns that agents inhibiting both mutant and wild-type HTT may induce serious side effects in HD patients, especially if chronic administration is necessary. One approach to distinguish mutant from wild-type alleles in HD and other neurological diseases involves siRNAs that target single-nucleotide or deletion polymorphisms[11–16]. But differences in polymorphisms between patients complicate routine clinical application of allele-specific RNA interference (RNAi).

To identify agents that block the neurodegenerative effects of the mutant gene while preserving the normal biological function of the wild-type allele, we tested whether single-stranded oligomers might discriminate between wild-type and mutant alleles based on differences in the lengths of the expanded mRNA sequences. Our rationale, based on the ability of triplet-repeat sequences within RNA to form hairpin structures (**Supplementary Fig. 1** online)[20], was that because the structures formed by wild-type and mutant mRNAs possess different energies and stabilities, they might enable selective recognition of the mutant allele and subsequent selective inhibition of mutant protein expression. These differences are likely to be subtle, but even small differences may be enough to achieve useful levels of discrimination. Alternatively, the expanded repeats create additional target sequence and more potential binding sites. For example, an allele with a wild-type repeat number of 20 would accommodate a maximum of three 20-base oligomers, whereas a mutant allele with 40 repeats would be large enough to accommodate six 20-base oligomers.

To test this hypothesis, we synthesized 19-base peptide nucleic acid (PNA)–peptide conjugates targeting HTT mRNA (**Supplementary**

[1]Departments of Pharmacology and Biochemistry and [2]Physiology, University of Texas Southwestern Medical Center at Dallas, Dallas, Texas, USA. [3]SIGMA-Aldrich Genopole Campus, Evry Cedex, France. [4]These authors contributed equally to this work. Correspondence should be addressed to D.R.C. (david.corey@utsouthwestern.edu).

Received 18 February; accepted 3 April; published online 3 May 2009; doi:10.1038/nbt.1539

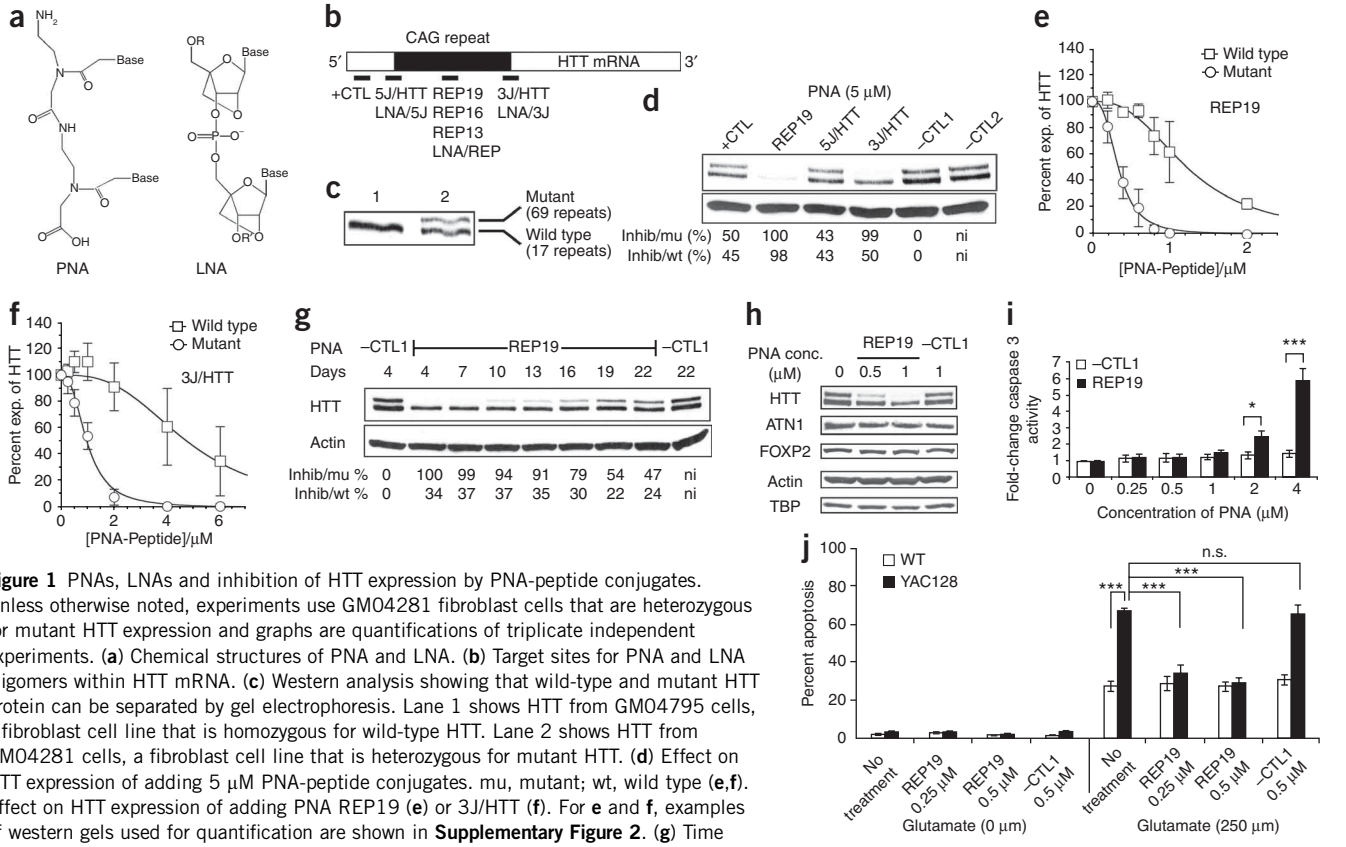

Figure 1 PNAs, LNAs and inhibition of HTT expression by PNA-peptide conjugates. Unless otherwise noted, experiments use GM04281 fibroblast cells that are heterozygous for mutant HTT expression and graphs are quantifications of triplicate independent experiments. (**a**) Chemical structures of PNA and LNA. (**b**) Target sites for PNA and LNA oligomers within HTT mRNA. (**c**) Western analysis showing that wild-type and mutant HTT protein can be separated by gel electrophoresis. Lane 1 shows HTT from GM04795 cells, a fibroblast cell line that is homozygous for wild-type HTT. Lane 2 shows HTT from GM04281 cells, a fibroblast cell line that is heterozygous for mutant HTT. (**d**) Effect on HTT expression of adding 5 μM PNA-peptide conjugates. mu, mutant; wt, wild type (**e**,**f**). Effect on HTT expression of adding PNA REP19 (**e**) or 3J/HTT (**f**). For **e** and **f**, examples of western gels used for quantification are shown in **Supplementary Figure 2**. (**g**) Time course of inhibition of HTT expression by PNA REP19 (1 μM). (**h**) Effect of PNA REP19 on expression of other proteins with mRNAs that contain CAG repeats. (**i**) Effect of adding PNA REP19 on cell toxicity measured by monitoring levels of caspase 3. $*P < 0.05$, $***P < 0.001$ relative to negative control PNA/–CTL1. $n = 3$. (**j**) Glutamate-induced apoptosis of WT and YAC128 MSN. The fraction of TUNEL-positive is shown for WT (open bars) and YAC128 (filled bars) MSN. Experiments were repeated five times and data from a blinded cell count is shown. Data were evaluated using one-way analysis of variance. Statistical difference was considered to be significant if $P \leq 0.05$. n.s., not statistically significant.

Table 1 online and **Fig. 1a**,**b**) and examined PNA-mediated inhibition of HTT expression in GM04281 patient-derived fibroblast cells (wild-type *HTT* allele contains 17 repeats and mutant *HTT* allele contains 69 repeats) (**Fig. 1c**). PNAs are a class of DNA/RNA mimics with an uncharged amide backbone that facilitates recognition of target sequences within RNA structure[21]. Unless otherwise noted, PNA conjugates were synthesized to contain a cationic peptide D-Lys_8 at the C terminus to promote the import of PNAs into cells[22].

We targeted the CAG repeat region (REP19) and also the 5′ junction (5J/HTT) and the 3′ junction (3J/HTT) because complementarity to mRNA sequence outside the CAG repeat may further enhance the specificity for targeting mutant HTT mRNA relative to other cellular mRNAs. PNA conjugates REP19 (PNA REP19) and 3J/HTT (PNA 3J/HTT) inhibited expression of HTT protein (**Fig. 1d**) and were chosen for further analysis. Inhibition of mutant HTT expression by PNA REP19 and PNA 3J/HTT was characterized by IC_{50} values of 0.34 μM and 0.96 μM, respectively (**Fig. 1e**,**f** and **Supplementary Fig. 2** and **Supplementary Table 2** online) and 3.5-fold and fivefold selectivities (wild-type IC_{50}/mutant IC_{50}), respectively, 4 d after transfection. Inhibition decreased as we progressively adjusted the PNA target site downstream of that of HTT/3J, thereby gradually decreasing complementarity to the CAG repeat (**Supplementary Fig. 3** online). PNA REP19 selectively inhibited expression of mutant HTT relative to wild-type HTT for up to 22 d after a one-time addition to cells (**Fig. 1g**). Noncomplementary control PNAs CTL1 and –CTL2 did not inhibit HTT expression.

Many genes contain CAG repeats, including some that are essential for cellular function. At concentrations sufficient for selective inhibition of mutant HTT, addition of PNA REP19 did not affect expression of representative genes containing CAG repeats, including TATA box binding protein (TBP) (19 CAG repeats), ATN1 (15 CAG repeats), FOXP2 (40 consecutive glutamines encoded by mixed CAG and CAA codons), AAK1 (6 CAG repeats) and POU3F2 (6 CAG repeats) (**Fig. 1h** and **Supplementary Fig. 4a** online) and did not cause cellular toxicity or affect rates of cell proliferation (**Supplementary Fig. 4b**). Cells began to exhibit toxic effects when PNA REP19 was added at concentrations ≥ 2 μM, a concentration almost fourfold greater than that required for allele-selective inhibition (**Fig. 1i** and **Supplementary Fig. 4c**).

To test the consequences of selectively inhibiting expression of mutant HTT protein on phenotypes related to HD, we added PNA REP19 to primary neuronal cell medium spiny neurons (MSN) cultures derived from YAC128 transgenic mice (**Fig. 1j** and **Supplementary Fig. 5** online)[23,24]. In this model, full-length human *HTT* mRNA containing 128 CAG repeats is expressed under control of its endogenous promoter in mice that also express wild-type murine HTT. MSN cells expressing mutant HTT protein are more susceptible to apoptosis upon addition of glutamate[24]. Addition of PNA REP19 to striatal cultures was neuroprotective against glutamate-induced toxicity, reducing the percentage of apoptotic YAC128 cells to ~30%, similar to levels seen in wild-type MSN. Although not a perfect mimic of the situation *in vivo* because it is an engineered transgene model

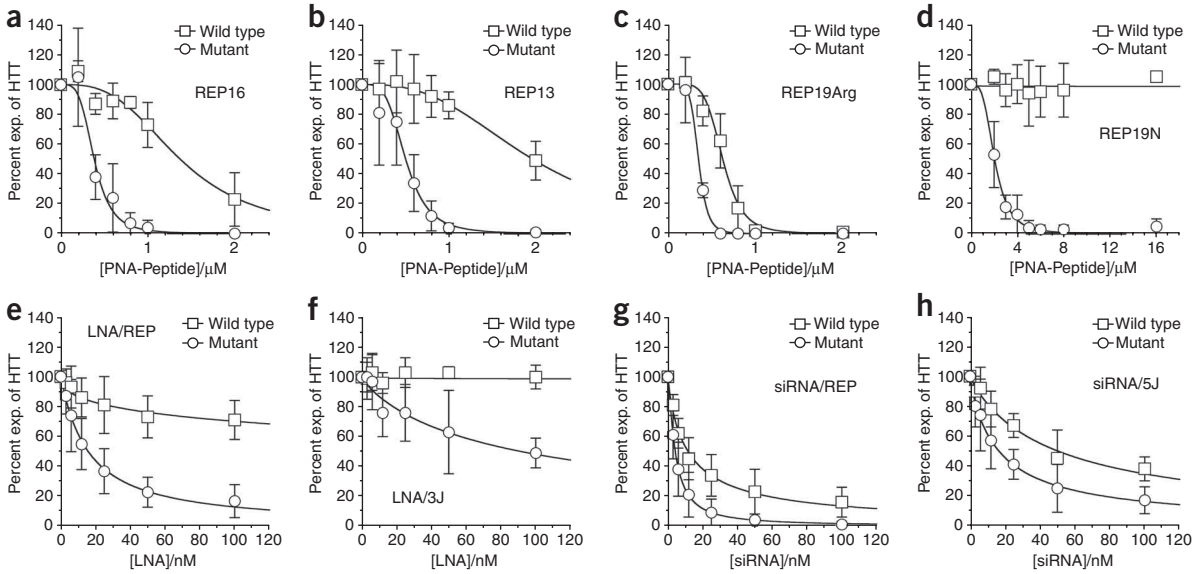

Figure 2 Effect of PNA modification, LNAs and siRNAs on selectivity. All quantification of western analysis of protein levels in GM04281 fibroblast cells is derived from at least three independent experiments. Examples of immunoblots used for quantification are shown in **Supplementary Figure 2**. (**a**–**h**) Effect on HTT expression of adding increasing concentrations of PNA REP16 (**a**), PNA REP13 (**b**), PNA REP19Arg (**c**), PNA REP19N (**d**), LNA/REP (**e**), LNA/3J (**f**), siRNA/REP (**g**) and siRNA/5J (**h**).

with mutant human *HTT* expression along with two wild-type mouse *htt* alleles, this experiment offers a first indication that the strategy may exert a protective effect in neuronal cells.

The PNAs are complementary to both mRNA and chromosomal DNA and could, in theory, block transcription by binding to *HTT* DNA. It is known that the binding of PNAs to mRNA does not reduce mRNA levels[25]. By contrast, the binding of PNAs to DNA blocks transcription and reduces mRNA levels[26]. We observed that addition of PNA REP19 did not decrease levels of *HTT* mRNA (monitored by quantitative PCR) or alter levels of RNA polymerase 2 at the *HTT* promoter (monitored by chromatin immunoprecipitation) (**Supplementary Fig. 6** and **Supplementary Methods** online). Indeed, efficient inhibition of both *HTT* alleles increased levels of *HTT* mRNA by a mechanism that does not involve enhancing the stability of *HTT* mRNA. These data are consistent with a mechanism of our allele-selective PNAs binding to mRNA and blocking translation rather than binding to DNA and inhibiting transcription.

Given the many options for improving the activity of antisense oligonucleotides through changing their lengths or introducing chemical modifications, we attempted to optimize allele-selective inhibition by varying PNA length and peptide conjugation. PNA-peptide conjugates that were 16 and 13 bases in length (PNA REP16 and PNA REP13, respectively) were potent and selective inhibitors with IC_{50} values of 0.39 μM and 0.47 μM, respectively (**Fig. 2a**,**b** and **Supplementary Fig. 2**). PNA REP13 did not affect expression of other proteins when used at 1 μM (**Supplementary Fig. 7** online). These results suggest that shorter PNAs can achieve potent and selective inhibition and broaden the options for designing effective agents.

A simple chemical modification to PNAs is replacement of D-arginine for D-lysine in the attached peptide. PNA REP19Arg was as potent an inhibitor (0.33 μM) as PNA REP19 attached to D-Lys_8 (0.34 μM), but selectivity for the mutant allele relative to the wild-type allele was reduced (1.9-fold for PNA REP19Arg versus 3.5-fold for PNA REP19) (**Fig. 2c**, **Supplementary Fig. 2** and **Supplementary Table 2**). This demonstrates that the composition of the peptide sequence affects selectivity for inhibition of mutant versus wild-type protein. The importance of cationic peptide sequence for recognition is not surprising; we have previously documented examples where replacement of an attached peptide that contains lysine with an analogous peptide that contains arginine substantially alters recognition of complementary nucleic acids[27].

Another straightforward modification is attachment of the peptide domain to the N rather than the C terminus of the PNA to afford PNA REP19N. In contrast to results showing lower selectivity with PNA REP19Arg relative to PNA REP19, PNA REP19N showed greater selectivity than PNA REP19. The IC_{50} value for inhibiting mutant HTT expression was 2.1 μM, with relatively no obvious inhibition of wild-type HTT at concentrations as high as 16 μM (**Fig. 2d** and **Supplementary Fig. 2**). This experiment demonstrates that improved selectivity can be achieved by varying conjugate design. We observed no inhibition of other proteins and only mild toxicity (**Supplementary Fig. 7**).

In contrast to PNAs, which have a neutral amide backbone, oligonucleotides have negatively charged phosphodiester backbones. Because of this basic difference in their chemical properties relative to PNAs, oligonucleotides will have a much different potential for developing antisense oligomers for therapy. Oligonucleotides are approved drugs and are being used in several clinical trials, and this clinical experience may offer practical advantages for their development for treating HD.

To explore whether this difference in chemical properties might influence the capacity for allele-selective inhibition, we tested single-stranded oligonucleotides that contain locked nucleic acid (LNA) bases[28]. LNA is an RNA analog that contains a methylene bridge between the 2′-O and 4′-C of the ribose (**Fig. 1a**). LNA bases can be placed at any position and allow the thermal stability of oligonucleotides to be precisely tailored for any application. In contrast to the neutral amide backbone of PNAs, LNAs have a negatively charged phosphodiester backbone, allowing us to use cationic lipid to introduce LNAs into cells. LNA oligomers are being tested in clinical trials[28].

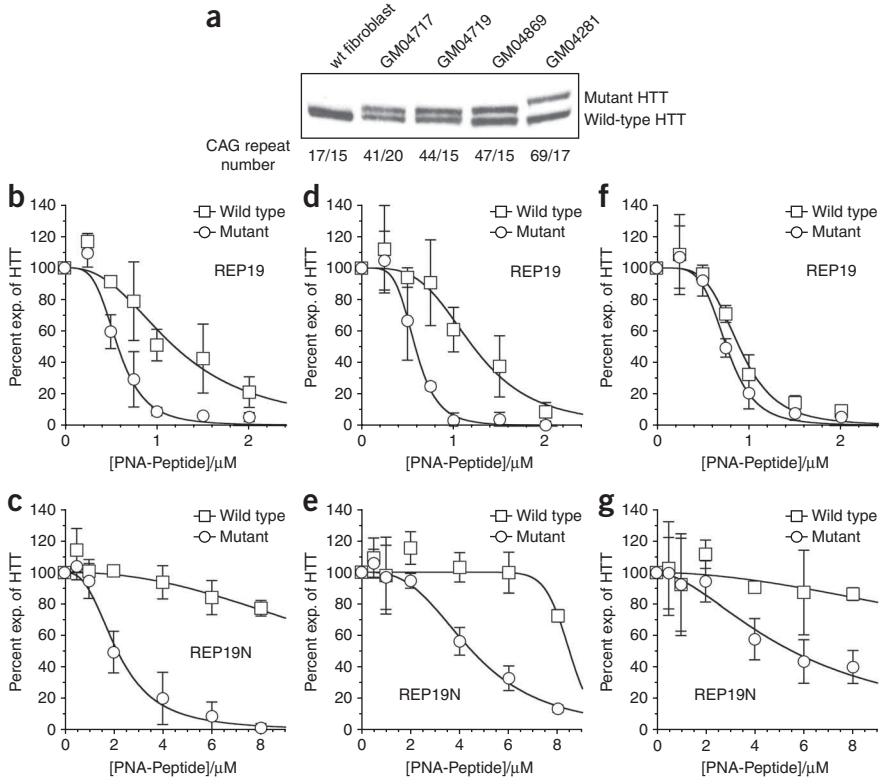

Figure 3 Selectivity is affected by the number of repeats in mutant HTT. All quantification of protein levels in fibroblast cells by western analysis is derived from at least three independent experiments. Examples of immunoblots used for quantification are shown in **Supplementary Figure 9**. (**a**) Separation by SDS-PAGE of wild-type and mutant HTT protein variants in four different patient-derived cell lines. The first number is the number of repeats in the mutant allele, the second number is the number of repeats in the wild-type allele. (**b**–**g**) Effect on HTT protein expression of adding REP19 to GM04869 cells (**b**), REP19N to GM04869 cells (**c**), REP19 to GM04719 cells (**d**), REP19N to GM04719 cells (**e**), REP19 to GM04717 cells (**f**) and REP19N to GM04717 cells (**g**).

We observed allele-selective inhibition of mutant HTT expression by LNA/REP or LNA/3J (**Fig. 2e**,**f** and **Supplementary Fig. 8a** online). Inhibition by LNA/REP and LNA/3J was characterized by IC_{50} values of 0.017 and 0.086 μM, respectively (**Supplementary Fig. 2** and **Supplementary Table 2**). These IC_{50} values are lower than those achieved using PNA-peptide conjugates, but because the transfection protocols differ, it is impossible to draw direct conclusions regarding relative potencies. Inhibition of wild-type HTT was ≤30% at 100 nM, the maximum concentration tested. Concentrations of LNA that selectively blocked expression of mutant HTT did not affect other genes that contain CAG repeats (**Supplementary Fig. 8b**). LNA/REP caused a modest decrease in levels of HTT mRNA relative to noncomplementary LNA controls (**Supplementary Fig. 8c**). In contrast to PNAs, LNAs that contain LNA bases spread throughout a DNA backbone form DNA:RNA hybrids upon binding to mRNA and can recruit RNase H[29]. The resultant cleavage may explain the observed lower levels of mRNA.

The potency and widespread use of duplex RNAs (siRNAs)[30] make them a good benchmark for evaluating the effectiveness of PNAs and LNAs. To test whether siRNAs would also achieve selective inhibition of mutant HTT, we introduced duplex RNAs analogous in sequence to PNA REP19, PNA 5J/HTT and PNA 3J/HTT into GM04281 fibroblast cells. Like LNAs, and unlike PNA-peptide conjugates, siRNAs have a phosphodiester backbone and we used cationic lipid to assist their entry into cells. We observed inhibition of HTT expression by siRNA/REP and siRNA/5J (**Fig. 2g**,**h**, **Supplementary Fig. 2**) characterized by IC_{50} values of 0.005 and 0.018, respectively (**Supplementary Table 2**). siRNA/REP revealed a narrow window for selectivity with relatively low statistical significance (**Fig. 2g**), whereas siRNA/5J exhibited a selectivity of approximately threefold (**Fig. 2h** and **Supplementary Table 2**). Our RNAs were not chemically modified and duplex RNAs with well-chosen modifications might achieve better selectivity.

Most HD patients have mutant mRNAs with 40–50 CAG repeats[5]. We extended our studies to patient-derived fibroblast cell lines GM04869 (wild-type allele, 15 repeats; mutant allele, 47 repeats), GM04719 (wild-type allele, 15 repeats; mutant allele, 44 repeats) and GM04717 (wild-type allele, 20 repeats; mutant allele, 41 repeats) (**Fig. 3**). Upon addition of PNA REP19 to cells, we observed inhibition of mutant HTT in GM04869 (**Fig. 3b**), GM04719 (**Fig. 3d**) and GM04717 (**Fig. 3f**) cells with selectivities (wild-type IC_{50} value/mutant IC_{50} value) of 2.1, 1.8 and 1.2, respectively (**Supplementary Fig. 9** and **Supplementary Table 2** online), values reduced relative to the 3.5-fold selectivity achieved in GM04281 cells (**Fig. 1e**). We observed slight decreases in the potency of inhibition of mutant HTT as the number of mutant repeats was decreased from 47 to 44 and 41. The observation that the most potent inhibition of wild-type HTT occurred in the cell line (GM04717) with the most repeats in the wild-type allele is consistent with a correlation between the number of repeats and susceptibility to inhibition by PNA REP19. However, additional experiments are needed to better evaluate this hypothesis.

Because we had previously observed that attachment of the D-Lys_8 peptide to the PNA N terminus improves selectivity in GM04281 cells (**Fig. 2d**), we tested N-linked conjugate PNA REP19N in the cell lines that possess mutant alleles with fewer CAG repeats. We observed inhibition of mutant HTT in GM04869 (**Fig. 3c**), GM04719 (**Fig. 3e**) and GM04717 (**Fig. 3g**) cells with selectivities (wild-type IC_{50} value/mutant IC_{50} value) of >3.5, >1.8 and >1.5, respectively (**Supplementary Fig. 9** and **Supplementary Table 2**). These data suggest that simple chemical modifications could potentially extend allele-selective inhibition of HTT protein expression to a broader subset of HD patients.

We selected *ATXN3*, the gene in which a CAG repeat expansion causes MJD[2], as a target to test whether allele-selective inhibition could be achieved with other genes containing repeats. To examine the potential for allele-specific inhibition in MJD cells, we obtained patient-derived cell line GM06151, which is heterozygous for an expanded CAG repeat (wild-type allele, 24 repeats; mutant allele, 74 repeats). The 74 repeats of the mutant allele fall within the middle of the range of repeat numbers found in patient samples[31].

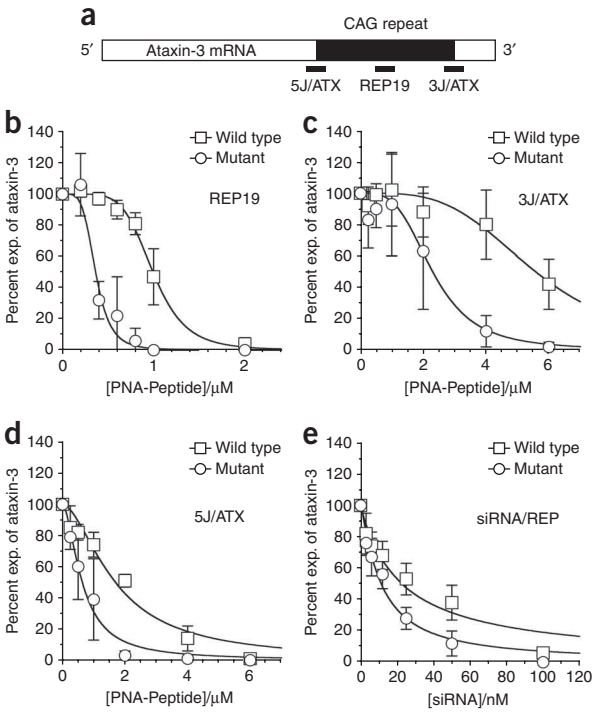

Figure 4 Potent and selective inhibition of mutant ataxin-3 in GM06151 fibroblasts. Examples of immunoblots used for quantification are shown in **Supplementary Figure 10**. (**a**) Target sites for PNAs within ataxin-3 mRNA. (**b**–**e**) Inhibition of ataxin-3 expression by (**b**) PNA REP19, (**c**) PNA 3J/ATX, (**d**) PNA 5J/ATX and (**e**) siRNA/REP.

We tested PNA conjugates that targeted the CAG repeat region (PNA REP19), the 5′ junction (PNA 5J/ATX), and the 3′ junction (PNA 3J/ATX) (**Fig. 4a**, **Supplementary Fig. 10** and **Supplementary Table 2** online). PNA REP19 selectively inhibited expression of mutant ataxin-3 with an IC_{50} value of 0.36 μM (**Fig. 4b**). Conjugates that target the 5′ and 3′ junctions also caused selective inhibition, with IC_{50} values of 0.7 μM and 2.2 μM, respectively (**Fig. 4c**,**d**). These data suggest that our strategy can be extended beyond HTT to other therapeutic targets. We also tested siRNA/REP. Similar to our observations for inhibition of HTT protein expression (**Fig. 2**), this siRNA was an inhibitor of ataxin-3 expression but yielded less-selective reduction of the mutant protein than did PNA REP19 (**Fig. 4e**). A failure of a repeat-targeted siRNA to selectively inhibit ataxin-3 expression had been reported previously[11].

One obstacle to therapy for HD or MJD will be delivery to the central nervous system because oligonucleotides are not distributed to the brain after intravenous or oral administration. Single-stranded oligonucleotides can be delivered directly to the central nervous system and block gene expression[32]. Although LNAs have not been used in animal models of HD or MJD, they have been administered into rodent brains by several methods (intrathecal, intracerebroventricular and intrastriatal)[33,34]. Toxicity is minimal and potent inhibitory effects were observed for targeting deltorphin II[33] and miRNA-21 (ref. 34).

Much attention has been focused on allele-selective inhibition using siRNAs complementary to sequences that have single-nucleotide or deletion polymorphisms[11–16]. Although an advantage of this approach is that it involves familiar RNAi technology, the diversity of polymorphisms within patient populations would necessitate developing multiple siRNAs. Even then, this approach, based on single-nucleotide polymorphisms, is unlikely to benefit patients like the one from whom our benchmark patient-derived cell line GM04281, which has none of the most commonly identified polymorphisms[14], was derived. We were able to perform experiments in GM09197 cells that have a deletion polymorphism and have been used to observe siRNA-mediated allele-selective inhibition[16]. LNA/REP offered better selectivity than the best allele-selective RNA (**Supplementary Fig. 11** online).

Patient populations are heterogeneous and approaches that target polymorphisms, triplet repeats or make no attempt at allele-selectivity may benefit different groups of patients. One advantage is that our approach uses one oligomer strand rather than the two needed for siRNAs, simplifying issues associated with clinical development such as compound synthesis and the potential for off-target effects. Conversely, although we demonstrate that optimizing the structure of the oligomer can lead to better selectivity over a wide range of repeats, it may be difficult, using our strategy, to achieve adequate selectivity for patients with shorter repeats.

Another important issue is the minimum efficacy sufficient for successful application *in vivo*. Complete inhibition of mutant protein expression might not be necessary to achieve beneficial therapeutic effects; even partial reduction of mutant protein levels may be adequate. Conversely, partial inhibition of wild-type protein may not have adverse consequences because the remaining wild-type protein may be sufficient for function. The window for therapy may be relatively broad, requiring less than complete inhibition of mutant protein expression and tolerating partial reduction in wild-type protein levels. Such information will help set the therapeutic window for drug development.

Given that the allele-selective inhibition of HTT and ataxin-3 occurs intracellularly, it is difficult to assign an exact molecular mechanism to the effects we have observed. Clearly, some complementarity to the CAG repeat is essential, because potency is lost when downstream regions are targeted (**Supplementary Fig. 3**). Although the number of oligomers bound to the mutant and wild-type expanded repeats may contribute to selectivity, our evidence involving different PNAs, LNAs and siRNAs is consistent with a mechanism that at least partially involves an ability of PNAs and LNAs to sense structural differences between extended repeats in the cell. Addition of PNAs does not reduce levels of mRNA or recruitment of RNA polymerase 2 to the *HTT* promoter (**Supplementary Fig. 6**), consistent with a steric blocking mechanism in which the PNA binds to mRNA rather than DNA. This 'steric blocking' mode of action for antisense PNAs was expected based on previous studies of PNAs complementary to mRNA[25].

Our findings offer two lessons. The first is that single-stranded oligomers can discriminate among sequences inside cells on the basis of context—in this case the length of a polyglutamine tract and the potential of different repeat lengths to form energetically different structures—rather than base differences. The second is that the potential for developing single-stranded oligomers as allele-selective treatment for genetic disease is greater than had been appreciated previously. There is broad potential for optimizing the selectivity and potency of our most promising candidates. Antisense oligomers for other diseases are making good progress in clinical trials[35] and appear to offer near-term potential for wider therapeutic application. Exploiting the ability of antisense oligomers to selectively recognize mutant nucleic acid sequences offers a promising strategy for developing therapies for HD, MJD and other triplet-repeat disorders.

METHODS

Cell culture and transfection. PNA-peptide conjugates were synthesized and purified as desccribed[22,26]. LNA oligonucleotides were provided by Sigma-Aldrich. siRNAs were purchased from Integrated DNA Technologies (IDT). Patient-derived fibroblast cell lines GM04281, GM06151, GM04719, GM04869, GM04717, GM04795 and GM09197 were obtained from the Coriell Institute. Cells were maintained at 37 °C and 5% CO_2 in MEM (Sigma) supplemented with 10% heat inactivated FBS (Sigma) and 0.5% MEM nonessential amino acids (Sigma). Cells were plated in 6-well plates at 60,000 cells/well in supplemented MEM 2 d before transfection. Stock solutions of PNA-peptide conjugates were heated at 65 °C for 5 min before use to dissolve any aggregates that may have formed. PNA-peptide conjugates were diluted to the appropriate concentration using OptiMEM (Invitrogen) and then added to cells. After 24 h, the media containing PNA-peptides were removed and replaced by fresh supplemented MEM. Unless indicated otherwise, cells were harvested 4 d after transfection for protein assay. siRNAs or LNAs were transfected to cells using RNAiMAX (Invitrogen) according to the manufacturer's instructions. The appropriate amount of the lipid (3 µl for 100 nM oligonucleotides) was added to OptiMEM containing oligonucleotides and the oligonucleotide-lipid mixture (250 µl) was incubated for 20 min. OptiMEM was added to the mixture to a final volume of 1.25 ml and then added to cells. The media were exchanged 24 h later with fresh supplemented MEM.

Analysis of HTT and ataxin-3 expression. Cells were harvested with trypsin-EDTA solution (Invitrogen) and lysed. The protein concentration in each sample was quantified with bicinchoninic acid (BCA) assay (Thermo Scientific). SDS-PAGE (separating gel: 5% acrylamide-bisacrylamide/34.7:1, 450 mM Tris-acetate pH 8.8; stacking gel: 4% acrylamide-bisacrylamide/34.7:1, 150 mM Tris-acetate pH 6.8) (XT Tricine Running Buffer, Bio-Rad) was used to separate WT and mutant HTT proteins (**Supplementary Figs. 12** and **13** online). Gels were run at 70 V for 15 min followed by 100 V for 4 h. For separation of HTT variants containing shorter CAG repeats, gels were run at 70 V for 15 min, then 110 V for 6 h. The electrophoresis apparatus was placed in an ice-water bath to prevent overheating of the running buffer. We monitored expression of actin protein to ensure even loading on protein in each lane. In parallel with analysis for HTT expression, portions of each protein lysate sample were analyzed for β-actin expression by SDS-PAGE (7.5% acrylamide pre-cast gels; Bio-Rad). These gels were run at 70 V for 15 min followed by 100 V for 1 h. After gel electrophoresis, proteins were transferred to membrane (Hybond-C Extra; GE Healthcare Bio-Sciences). Ataxin-3 and β-actin were analyzed by SDS-PAGE (7.5% acrylamide pre-cast gels; Bio-Rad). Primary antibodies specific for each protein were obtained and used at the indicated dilution ratio: anti-HTT antibody (MAB2166; 1:10,000; Chemicon), anti-ataxin-3 antibody (MAB5360; 1:10,000; Chemicon), and anti-β-actin antibody (1:10,000; Sigma).

HRP conjugate anti-mouse or anti-rabbit secondary antibody (1:10,000 and 1:5,000, respectively; Jackson ImmunoResearch Laboratories) was used for visualizing proteins using SuperSignal West Pico Chemiluminescent Substrate (Thermo Scientific). Protein bands were quantified using ImageJ software. The percentage of inhibition was calculated as a relative value to a control sample.

Neuronal cell glutamate susceptibility assay[23,24]. YAC128 mice (FVBN/NJ background strain) were obtained from Jackson Labs. The male YAC128 mice were crossed to WT female FVBN/NJ mice and P1-P2 pups were collected and genotyped by PCR. The primary cultures of striatal MSN were established from YAC128 and control WT pups. Striata were dissected, diced and digested with trypsin. After dissociation, neurons were plated on poly-L-lysine (Sigma)-coated 12-mm round coverslips (Assistent) in Neurobasal-A medium supplemented with 2% B27, 1 mM glutamine and penicillin-streptomycin (all from Invitrogen) and kept at 37 °C in a 5% CO_2 environment. PNA was added to the 9-days-*in-vitro* (DIV) MSN. The 13-DIV MSN were exposed for 7 h to 250 µM glutamate in Neurobasal-A added to the culture medium. Immediately after the treatment with glutamate, neurons were fixed for 30 min in 4% paraformaldehyde plus 4% sucrose in PBS (pH 7.4), permeabilized for 5 min in 0.25% Triton-X-100 and stained by using the DeadEnd fluorometric TUNEL System (Promega). Nuclei were counterstained with 5 µM propidium iodine (PI) (Molecular Probes). Coverslips were extensively washed with PBS and mounted in Mowiol 4-88 (Polysciences). For quantification six to eight randomly chosen microscopic fields, each containing 100–300 MSN, were counted for YAC128 and WT cultures. The number of TUNEL-positive neuronal nuclei was calculated as a fraction of PI-positive neuronal nuclei in each microscopic field. The fractions of TUNEL-positive nuclei determined for each microscopic field were averaged and the results are presented as means ± s.e.m. (n = number of fields counted). MSN cells were supported in culture by surrounding glial cells, but only MSN cells were counted during the neuroprotection assay.

PNA REP19 was added at the concentration of 0.25 µM and 0.5 µM, 4 d before the glutamate application. Noncomplementary PNA –CTL1 was added at 0.5 µM. MSN were exposed to 250 µM glutamate at 13-DIV for 7 h, fixed, permeabilized and analyzed by TUNEL staining and PI counterstaining. The data are presented as mean ± s.e.m. (n = 6–8 microscopic fields, 100–300 MSN per field).

For protein assays, after the addition of PNA REP19 at 9-DIV, the 13-DIV MSN were washed with ice-cold PBS and solubilized for 30 min at 4 °C in extraction buffer A (1% CHAPS, 137 mM NaCl, 2.7 mM KCl, 4.3 mM Na_2HPO_4, 1.4 mM KH_2PO_4 (pH 7.2), 5 mM EDTA, 5 mM EGTA and protease inhibitors). Extracts were clarified by centrifugation for 20 min at 10,000*g* at 4 °C and the upper solutions were collected for SDS-PAGE. For selectively harvesting MSN, cells were incubated with cell dissociation solution (Sigma) for 4 min at 37 °C and neuron basal-A medium with 10% FBS were added. MSN were detached from plate and most of the glial cells were not harvested. The combined solution was collected and lysed as previously described[23,24].

Caspase-3 activity assay. Caspase-3 activity was measured by hydrolysis of acetyl-Asp-Glu-Val-Asp p-nitroanilide (Ac-DEVD-pNA) according to the manufacturer's instruction in a colorimetric assay kit (Sigma). Fibroblast cells in 6-well plate were harvested as previously described. The cell pellet was resuspended in 15 µl of 1× lysis buffer without protease inhibitor and incubated for 30 min on ice. Protein concentration was determined by BCA assay (Thermo Scientific). We mixed 50 µg of cell extract with 2 mM Ac-DEVD-pNA substrate to a total volume of 100 µl of 1× assay buffer in a 96-well plate and incubated at 37 °C overnight. The absorbance was read at 405 nm.

Analysis of *TBP, AAK1, ATN1, FOXP2* and *POU3F2*. The number of CAG repeats was estimated according to the published mRNA sequence in GenBank. TATA box binding protein (*TBP*) (~19 CAG repeats, NM_003194), *AAK1* (6 CAG repeats, NM_014911), *ATN1* (15 CAG repeats, NM_001940), *FOXP2* (~40 CAA···CAG repeats, NM_148899) and *POU3F2* (~6 CAG repeats, NM_005604). Protein lysates were analyzed by SDS-PAGE (7.5% acrylamide pre-cast gels; Bio-Rad) followed by western blotting with anti-TBP antibody (1:2,000; Sigma), anti-AAK1 antibody (1:1,000; Abcam), anti-ATN1 antibody (1:300; Affinity Bioreagents), anti-FOXP2 antibody (1:1,000; Abcam) or anti-POU3F2 antibody (1:1,000; Abnova) (**Supplementary Fig. 13**).

Statistical analysis and curve fitting. Student t-test was performed for evaluating statistical significance between two study groups. Each data plot from dose response experiments for inhibition of HTT or ataxin-3 was fit to the following model equation, $y = 100(1\text{-}x^m/(n^m+x^m))$, where y is percent inhibition of protein and x is concentration of synthetic oligomers. m and n are fitting parameters, where n is taken as the IC_{50} value.

Note: Supplementary information is available on the Nature Biotechnology website.

ACKNOWLEDGMENTS

This work was supported by the High-Q Foundation, the US National Institutes of Health (NIGMS 60642 and 73042 to D.R.C.; NINDS RO1NS056224 to I.B.; NIBIB EB 05556 to J.C.S.), and the Robert A. Welch Foundation (I-1244 and I-1336) and Ataxia MJD research project. We thank B. Janowski for helpful comments and Y. Li for help maintaining the YAC128 mouse colony.

AUTHOR CONTRIBUTIONS

J.H. and M.M. designed and performed experiments in patient-derived fibroblast cells. J.W. and J.H. designed and performed experiments in MSN cells.

K.T.G. and J.C.S assisted with experiments. K.A. and S.G. supplied LNAs. D.R.C. and I.B. supervised experiments.

COMPETING INTERESTS STATEMENT

The authors declare competing financial interests: details accompany the full-text HTML version of the paper at http://www.nature.com/naturebiotechnology/

Published online at http://www.nature.com/naturebiotechnology/
Reprints and permissions information is available online at http://npg.nature.com/reprintsandpermissions/

1. Orr, H.T. & Zoghbi, H.Y. Trinucleotide repeat disorders. *Annu. Rev. Neurosci.* **30**, 575–621 (2007).
2. Paulson, H.L. Dominantly inherited ataxias: Lessons learned from Machado-Joseph disease/spinocerbeller ataxia type 3. *Semin. Neurol.* **27**, 133–142 (2007).
3. Walker, F.O. Huntington's disease. *Lancet* **369**, 218–228 (2007).
4. Gusella, J.F. & MacDonald, M.E. Huntington's disease: seeing the pathogenic process through a genetic lens. *Trends Biochem. Sci.* **31**, 533–540 (2006).
5. Kremer, B. *et al.* A worldwide study of the Huntington's disease mutation: The sensitivity and specificity of measuring CAG repeats. *N. Engl. J. Med.* **330**, 1401–1406 (1994).
6. Boado, R.J., Kazantsev, A., Apostol, B.L., Thompson, L.M. & Pardridge, W.M. Antisense-mediated down-regulation of the mutant human huntingtin gene. *J. Pharmacol. Exp. Ther.* **295**, 239–243 (2000).
7. Harper, S.Q. *et al.* RNA interference improves motor and neuropathological abnormalities in a Huntington's disease mouse model. *Proc. Natl. Acad. Sci. USA* **102**, 5820–5825 (2005).
8. Denovan-Wright, E.M. & Davidson, B.L. RNAi: a potential therapy for the dominantly inherited nucleotide repeat diseases. *Gene Ther.* **13**, 525–531 (2006).
9. Wang, Y.-L. *et al.* Clinico-pathological rescue of a model mouse of Huntington's disease by siRNA. *Neurosci. Res.* **53**, 241–249 (2005).
10. DiFiglia, M. *et al.* Therapeutic silencing of mutant huntingtin with siRNA attenuates striatal and cortical neuropathology and behavioral deficits. *Proc. Natl. Acad. Sci. USA* **104**, 17204–17209 (2007).
11. Miller, V.M. *et al.* Allele-specific silencing of dominant disease genes. *Proc. Natl. Acad. Sci. USA* **100**, 7195–7200 (2003).
12. Schwarz, D.S. *et al.* Designing siRNA that distinguish between genes that differ by a single nucleotide. *PLoS Genet.* **2**, e140 (2006).
13. Rodriguez-Lebron, E. & Paulson, H.L. Allele-specific RNA interference for neurological disease. *Gene Ther.* **13**, 576–581 (2006).
14. van Bilsen, P.H.J. *et al.* Identification and allele-specific silencing of the mutant huntingtin allele in Huntington's disease patient-derived fibroblasts. *Hum. Gene Ther.* **19**, 710–718 (2008).
15. Alves, S. *et al.* Allele-specific RNA silencing of mutant ataxin-3 mediates neuroprotection in a rat model of Machado-Joseph disease. *PLoS One* **3**, e3341 (2008).
16. Zhang, Y., Engelman, J. & Friedlander, R.M.J. Allele-specific silencing of mutant Huntington's disease gene. *J. Neurochem.* **108**, 82–90 (2009).
17. De Souza, E.B., Cload, S.T., Pendergrast, P.S. & Sah, D.W. Novel therapeutic modalities to address nondrugable protein interaction targets. *Neuropsychopharmacology* **34**, 142–158 (2009).
18. Nasir, J. *et al.* Targeted disruption of the Huntington's disease gene results in embryonic lethality and behavioral and morphological changes in heterozygotes. *Cell* **81**, 811–823 (1995).
19. White, J.K. *et al.* Huntingtin is required for neurogenesis and is not impaired by the Huntington's disease CAG expansion. *Nat. Genet.* **17**, 404–410 (1997).
20. Sobczak, K., de Mezer, M., Michlewski, G., Krol, J. & Krzyzosiak, W.J. RNA structure of trinucleotide repeats associated with human neurological diseases. *Nucleic Acids Res.* **31**, 5469–5482 (2003).
21. Marin, V.L. & Armitage, B.A. RNA guanine quadruplex invasion by complementary and homologous PNA probes. *J. Am. Chem. Soc.* **127**, 8032–8033 (2005).
22. Hu, J. & Corey, D.R. Inhibiting gene expression with peptide nucleic acid (PNA)-peptide conjugates that target chromosomal DNA. *Biochemistry* **46**, 7581–7589 (2007).
23. Slow, E.J. *et al.* Selective striatal neuronal loss in a YAC128 mouse model for Huntington disease. *Hum. Mol. Genet.* **12**, 1555–1567 (2003).
24. Tang, T.-S. Disturbed Ca^{2+} signaling and apoptosis of medium spiny neurons in Huntington's disease. *Proc. Natl. Acad. Sci. USA* **102**, 2602–2607 (2005).
25. Knudsen, H. & Nielsen, P.E. Antisense properties of duplex- and triplex-forming PNAs. *Nucleic Acids Res.* **24**, 494–500 (1996).
26. Janowski, B.A. *et al.* Inhibiting transcription of chromosomal DNA with antigene peptide nucleic acids. *Nat. Chem. Biol.* **1**, 210–215 (2005).
27. Corey, D.R. 48,000-fold acceleration of hybridization of chemically modified oligonucleotides to duplex DNA. *J. Am. Chem. Soc.* **117**, 9373–9374 (1995).
28. Koch, T. *et al.* Locked nucleic acid: Properties and therapeutic aspects. in *Therapeutic Oligonucleotides* (ed. Kurreck, J.) 103–141, (RSC Biomolecular Sciences, Royal Society of Chemistry, Cambridge, UK, 2008).
29. Kurreck, J., Wyszko, E., Gillen, C. & Erdmann, V.A. Design of antisense oligonucleotides stabilized by locked nucleic acids. *Nucleic Acids Res.* **30**, 1911–1918 (2002).
30. Bumcrot, D., Manoharan, M., Koteliansky, V. & Sah, D.W. RNAi therapeutics: a potential new class of pharmaceutical drugs. *Nat. Chem. Biol.* **2**, 711–719 (2006).
31. Maruyama, H. *et al.* Molecular features of the CAG repeats and clinical manifestation of Machado-Joseph disease. *Hum. Mol. Genet.* **4**, 807–812 (1995).
32. Smith, R.A. *et al.* Antisense oligonucleotide therapy for neurodegenerative disease. *J. Clin. Invest.* **116**, 2290–2296 (2006).
33. Wahlestedt, C. *et al.* Potent and nontoxic antisense oligonucleotides containing locked nucleic acids. *Proc. Natl. Acad. Sci. USA* **97**, 5633–5638 (2000).
34. Corsten, M.F. *et al.* MicroRNA-21 knockdown disrupts glioma growth in vivo and displays synergistic cytotoxicity with neural precursor cell delivered S-TRAIL in human gliomas. *Cancer Res.* **67**, 8994–9000 (2007).
35. Corey, D.R. RNAi learns from antisense. *Nat. Chem. Biol.* **3**, 8–11 (2007).

Supplementary Table 1. PNA, duplex RNAs, and LNA oligomers used in these studies.

Name	Sequence (length)
PNA-peptide conjugates	
REP19	K-GCTGCTGCTGCTGCTGCTG-K_8 (19)
REP19N	K_8-GCTGCTGCTGCTGCTGCTG-K (19)
REP19Arg	K-GCTGCTGCTGCTGCTGCTG-R_8 (19)
REP16	K-GCTGCTGCTGCTGCTG-K_8 (16)
REP13	K-GCTGCTGCTGCTG-K_8 (13)
5J/HTT	K-GCTGCTGCTGGAAGGACTT-K_8 (19)
3J/HTT	K-GGCGGCTGTTGCTGCTGCT-K_8 (19)
+CTL	K-GCTTTTCCAGGGTCGCCAT-K_8 (19)
-CTL1	K-GCTATACCAGCGTCGTCAT-K_8 (19)
-CTL2	K_8-ACCTACTGTCCTCGGCACCA-K (20)
5J/ATX	K-GCTGCTGCTGTTGCTGCTT-K_8 (19)
3J/ATX	K-ATAGGTCCCGCTGCTGCTG-K_8 (19)
siRNAs	
siRNA/REP	GCUGCUGCUGCUGCUGCUGTT (21)
siRNA/5J	GCUGCUGCUGGAAGGACUUTT (21)
siRNA/3J	GGCGGCUGUUGCUGCUGCUTT (21)
siRNA/+CTL	GCUUUUCCAGGGUCGCCAUTT (21)
siRNA/-CTL	GCUAUACCAGCGUCGUCAUTT (21)
siRNA/S4	GAGGAAGAGGAGGAGGCCGACTT (23)
LNAs	
LNA/REP	gcTgcTgcTgcTgcTgcTg (19)
LNA/5J	gcTgcTgcTggAagGacTt (19)
LNA/3J	ggCggCtgTtgCtgCtgCt (19)
LNA/+CTL	gcTttTccAggGtcGccAt (19)
LNA/-CTL	gcTatAccAgcGtcGtcAt (19)

PNAs are listed N to C terminal. siRNAs (antiense strands only) and LNAs are listed 5' to 3'. D-amino acids are used in all peptide conjugates. K=lysine, R=arginine. Mismatched bases are underlined. For LNAs, modified bases are represented as capital letters and DNA bases are lower case.

Nature Biotechnology: doi: 10.1038/nbt.1539

Supplementary Table 2. IC_{50} values (μM) and statistical significance for inhibition of mutant and wild-type alleles of HTT and ataxin-3 in varied cell lines.

	Inhibition of HTT							
	GM04281		GM04869		GM04719		GM04717	
REP19/wt	1.2 ± 0.3	**	1.2 ± 0.4	*	1.2 ± 0.4	p=0.101	0.90 ± 0.07	*
REP19/mut	0.34 ± 0.03		0.58 ± 0.07		0.66 ± 0.22		0.76 ± 0.04	
REP19N/wt	> 16		> 8		> 8		> 8	
REP19N/mut	2.1 ± 0.5		2.3 ± 0.3		4.5 ± 0.4		5.4 ± 1.5	
3J/HTT/wt	4.8 ± 1.8	**	n.d.		n.d.		n.d.	
3J/HTT/mut	0.96 ± 0.13		n.d.		n.d.		n.d.	
REP16/wt	1.4 ± 0.3	**	n.d.		n.d.		n.d.	
REP16/mut	0.39 ± 0.11		n.d.		n.d.		n.d.	
REP13/wt	2.2 ± 0.4	***	n.d.		n.d.		n.d.	
REP13/mut	0.47 ± 0.18		n.d.		n.d.		n.d.	
REP19Arg/wt	0.64 ± 0.08	**	n.d.		n.d.		n.d.	
REP19Arg/mut	0.33 ± 0.04		n.d.		n.d.		n.d.	
LNA/REP/wt	> 0.1		n.d.		n.d.		n.d.	
LNA/REP/mut	0.017 ± 0.007		n.d.		n.d.		n.d.	
LNA/3J/wt	> 0.1		n.d.		n.d.		n.d.	
LNA/3J/mut	0.086 ± 0.038		n.d.		n.d.		n.d.	
siRNA/REP/wt	0.013 ± 0.005	p=0.069	n.d.		n.d.		n.d.	
siRNA/REP/mut	0.005 ± 0.003		n.d.		n.d.		n.d.	
siRNA/5J/wt	0.055 ± 0.023	*	n.d.		n.d.		n.d.	
siRNA/5J/mut	0.018 ± 0.010		n.d.		n.d.		n.d.	

	Inhibition of Ataxin-3	
	GM06151	
REP19/wt	0.99 ± 0.06	*
REP19/mut	0.36 ± 0.09	
3J/ATX/wt	5.4 ± 0.9	*
3J/ATX/mut	2.2 ± 1.1	
5J/ATX/wt	1.7 ± 0.3	*
5J/ATX/mut	0.7 ± 0.2	
siRNA/REP/wt	0.024 ± 0.009	*
siRNA/REP/mut	0.012 ± 0.004	

wt: IC_{50} value (μM) for inhibition of wild-type protein. mut: IC_{50} value (μM) for inhibition of mutant protein. Values represent means ± s.d. (n=3–6). * $p < 0.05$, ** $p < 0.01$, *** $p < 0.001$. n.d.=not determined.

Nature Biotechnology: doi: 10.1038/nbt.1539

Supplementary Methods

Analysis of HTT mRNA level by Quantitative PCR. Total RNA from treated and untreated fibroblast cells was extracted using TRIzol (Invitrogen) 3 days after transfection. Samples were then treated with DNase I at 25℃ for 10 min. Reverse transcription reactions were done using High Capacity Reverse Transcription Kit (Applied Biosystems) according to the manufacturer's protocol. Quantitative PCR was performed on a 7500 real-time PCR system (Applied Biosystems) using iTaq SYBR Green Supermix (Bio-rad). Data was normalized relative to levels of GAPDH mRNA. Primer sequences specific for HTT are as follows: forward primer, 5′–CGACAGCGAGTCAGTGAATG–3′; reverse primer, 5′–ACCACTCTGGCTTCACAAGG–3′. Primers specific for GAPDH were obtained from Applied Biosystems.

Chromatin immunoprecipitation (ChIP) of RNA polymerase 2 (RNAP2). GM04281 fibroblast cells used for ChIP were seeded at 1.8 million cells in 15 cm dishes. Two dishes were treated with mismatch-containing PNA –CTL1 and two with REP19. Transfections were performed as described above and cells were crosslinked with formaldehyde (1%) three days after transfection. Before crosslinking, a small sample was collected for western analysis. Cells were recovered by scraping and nuclei isolated. Nuclei were lysed in 1 mL lysis buffer (1% SDS, 10 mM EDTA, 50 mM Tris-HCl pH 8.1, 1x Roche protease inhibitors cocktail) and sonicated (2 pulses, 40% power, 30 sec). 100 μL of lysate was incubated overnight with 4 μg of monoclonal anti-RNAP2 antibody (Millipore 05-623) or mouse IgG negative control antibody (Millipore 12-371) diluted in 900 μL of immunoprecipitation Buffer (0.01% SDS, 1.1% Triton-X, 1.2 mM EDTA, 16.7 mM Tris pH 8.1, 167 mM NaCl, and 1x Roche protease inhibitors cocktail). Antibody was recovered with 60 μL of Protein A/G beads (Calbiochem EMD IP05). Beads were washed with low salt (0.1% SDS, 1% Triton-X, 2 mM EDTA, 20 mM Tris-HCl pH 8.1, 150 mM NaCl), high salt (see low salt but with 500 mM NaCl), LiCl solution

Nature Biotechnology: doi: 10.1038/nbt.1539

(0.25 M LiCl, 1% NP-40, 1% deoxycholate, 1 mM EDTA, and 10 mM Tris-HCl pH 8.1), and Tris-EDTA pH 8.0 (Ambion AM9863) washes. Protein was eluted with 500 μL of 1% SDS, 0.1M $NaHCO_3$ for 30 minutes at room temperature. Crosslinking was reversed by adding NaCl to 200 mM and heating at 65 ºC for at least 2 hours. Protein was digested by Proteinase K followed by extraction using an equal volume of phenol:chloroform:isoamyl alchohol and centrifugation. DNA in the aqueous layer was precipitated using 1/10 volume sodium acetate/ 2 volumes ethanol. The pellet was resuspended in 50 μL of nuclease-free water. Real time PCR was performed using Biorad iTaq SYBR® Supermix.

MTS assay. GM04281 fibroblast cells (5,000 cells/well) in 96-well plate were plated 1 day before transfection. The cells were transfected with PNA-peptides. On day 4, cell viability for each sample was measured using CellTiter 96® AQueous One Solution Cell Proliferation Assay Kit (Promega) according to the manufacturer's protocol.

Evaluation of HTT mRNA stability. M04281 fibroblast cells (60,000 cells/well) were plated and transfected. For no treatment samples (NT1 and NT2), the media were just changed with OptiMEM. One day after transfection, the media were removed and replaced by fresh supplemented MEM. On day 3, actinomycin D (5 μg/mL) was added to each sample except for NT1 to stop transcriptions. Each sample was harvested using TRIzol at the specific time points (0, 2, 4, and 6 h), and cDNAs were prepared for qPCR to measure HTT and GAPDH mRNA levels.

Western Analysis of HTT and ataxin-3 expression: blot preparation and cropping. For separation of HTT allelic variants, cell lysates from fibroblasts were loaded on 5% Tris-acetate gels. This type of gel is not commercially available and preparing by pouring acrylamide solution into empty Ready Gel cassettes (Bio-Rad). Gel formulation: separating gel, 5% acrylamide-bisacrylamide/34.7:1,450 mM Tris-acetate pH 8.8; stacking gel: 4% acrylamide-bisacrylamide/34.7:1, 150 mM Tris-acetate pH 6.8. The separating gel is about 4.5 cm in length.

Nature Biotechnology: doi: 10.1038/nbt.1539

Gels were run at 70V for 15 min followed by 100V for 4 h. The electrophoresis apparatus was placed in ice-water bath to prevent excess heating that prevents good separation of the HTT variants. Under these conditions, HTT protein migrates to the bottom of the gel. Proteins were transferred to Hybond-C Extra membrane (100V for 2.5 h). After Ponceau S staining to reveal the location of protein bands, the membrane was cut from 1.5 to 3.5 cm from the bottom (the 250 kD protein maker we use to measure the progress of the electrophoresis is run off the gel in most cases).

For separation of HTT variants containing shorter CAG repeats, gels were run at 70 V for 15 min, then 110 V for 6 h. After transfer to the membrane, the blot was cut 2 cm above the bottom. The cropped blot was incubated in 5% milk, then probed with anti-HTT antibody (MAB2166. 1:10,000; Chemicon).

We monitor β-actin expression as a loading control to allow us to normalize HTT levels during quantitation. In parallel with analysis for HTT expression, an equivalent portion of each protein lysate was analyzed for β-actin expression by 7.5% Tris-HCl pre-cast gels (Bio-Rad). These gels were run at 70 V for 15 min followed by 100 V for 1 h. After transferring to the membrane, the blot was probed by anti-β-actin antibody (1:10,000; Sigma). It is necessary to run a separate gel because actin protein (~42 kDa) migrates much faster than HTT and runs off the gels used to separate HTT allelic variants. Under the conditions used to analyze β-actin, HTT appears as one band with no separation between the variants.

Ataxin-3 was analyzed by SDS-PAGE (7.5% Tris-HCl pre-cast gels; Bio-Rad). After transferring to the membrane, the blot was probed with anti-ataxin-3 antibody (MAB5360; 1:10,000; Chemicon). After treating with western blot stripping buffer (Fisher), the blot was then re-probed for β-actin.

Nature Biotechnology: doi: 10.1038/nbt.1539

Supplementary Figures

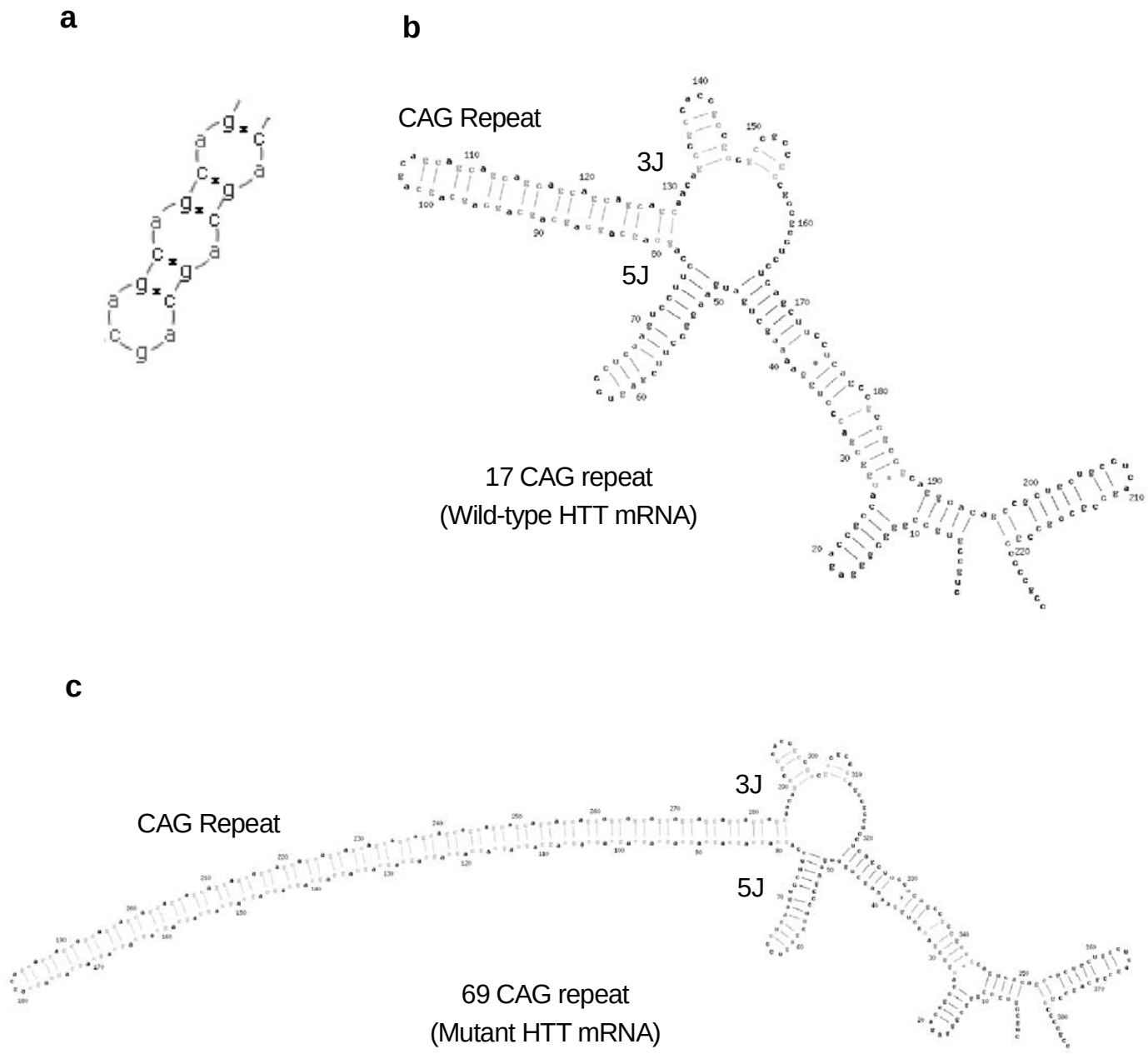

Supplementary Figure 1. Potential hairpin structures at CAG repeats. (**a**) Potential hairpin structure formed by CAG repeats. (**b, c**) CONTRAfold predictions of the structure of HTT mRNA with 17 (a typical number of wild-type repeats) or 69 (the number found in the mutant HTT allele of GM 04281 patient-derived fibroblast cells) CAG repeats respectively. The sequence is from base +121 ~ +360, NM_002111.

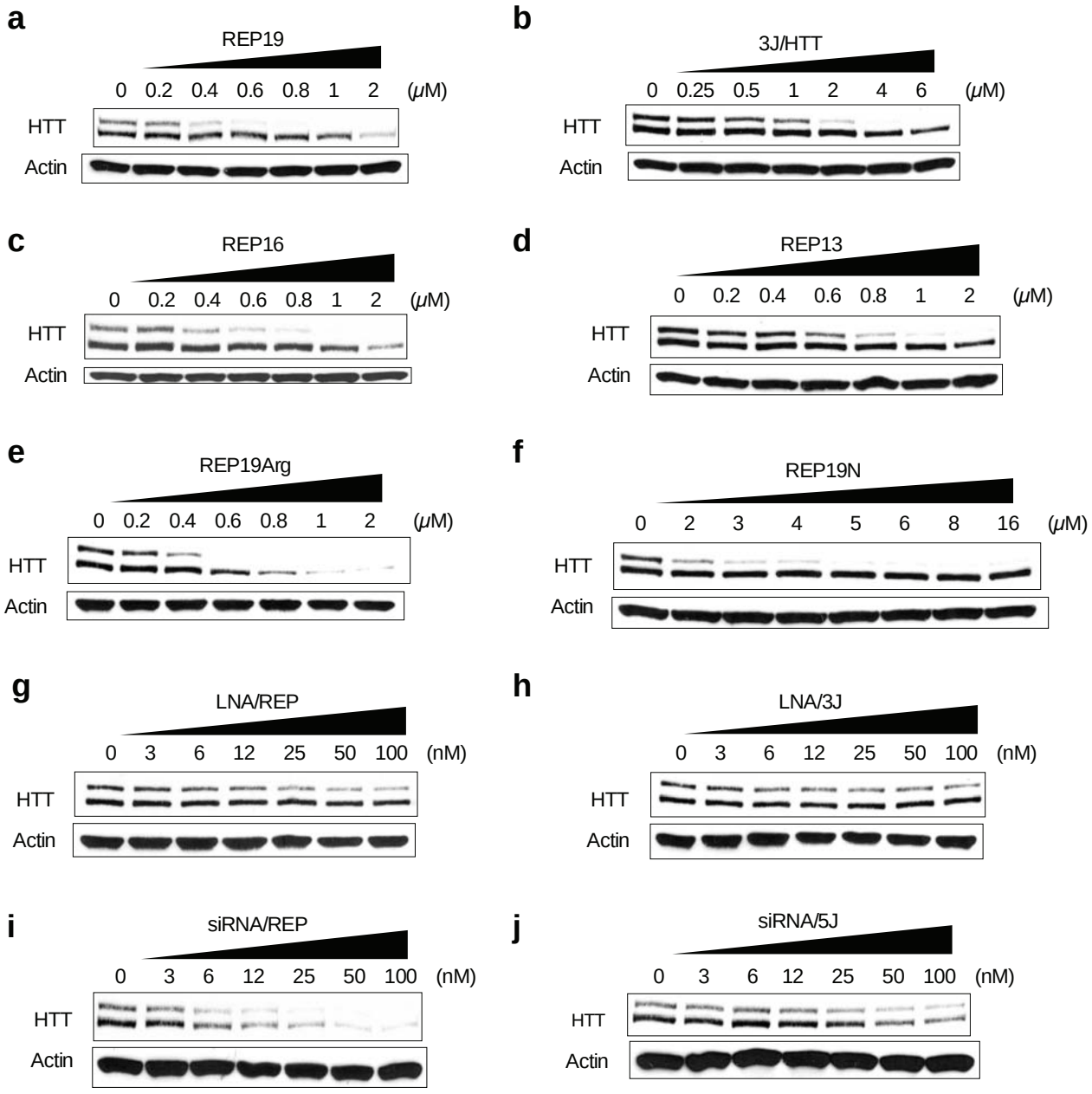

Supplementary Figure 2. Effect of oligomer concentration, target sequence, length and chemical modification: Western analysis. Typical western gels underlying the graphical data in Figures 1 and 2. Effect on HTT expression of adding increasing concentrations of (**a**) REP19, (**b**) 3J/HTT, (**c**) REP16, (**d**) REP13, (**e**) REP19Arg, (**f**) REP19N, (**g**) LNA/REP, (**h**) LNA/3J, (**i**) siRNA/REP and (**j**) siRNA/5J.

a

3J/HTT	K-GGCGGCTGTTGCTGCTGCT-K_8
3J10	K-CGGCTGTTGCTGCTGCTGC-K_8
3J6	K-GTGGCGGCTGTTGCTGCTG-K_8
3J4	K-CGGTGGCGGCTGTTGCTGC-K_8
3J0	K-GCGGCGGTGGCGGCTGTTG-K_8

b

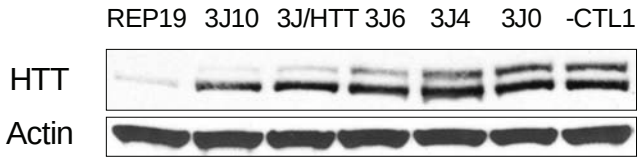

Supplementary Figure 3. **Inhibition of HTT protein expression by PNA conjugates that overlap the CAG/3' junction.** (**a**) Sequences of PNAs that are complementary to target sites that overlap the 3' junction between the CAG repeat and downstream regions of HTT mRNA. (**b**) Effect on HTT expression of adding 2 μM PNA conjugates 3J0, 3J4, 3J6, 3J/HTT, and 3J10 that target related sequences at the 3' junction and have 0, 4, 6, 8, and 10 bases of overlap with the CAG repeat respectively.

Nature Biotechnology: doi: 10.1038/nbt.1539

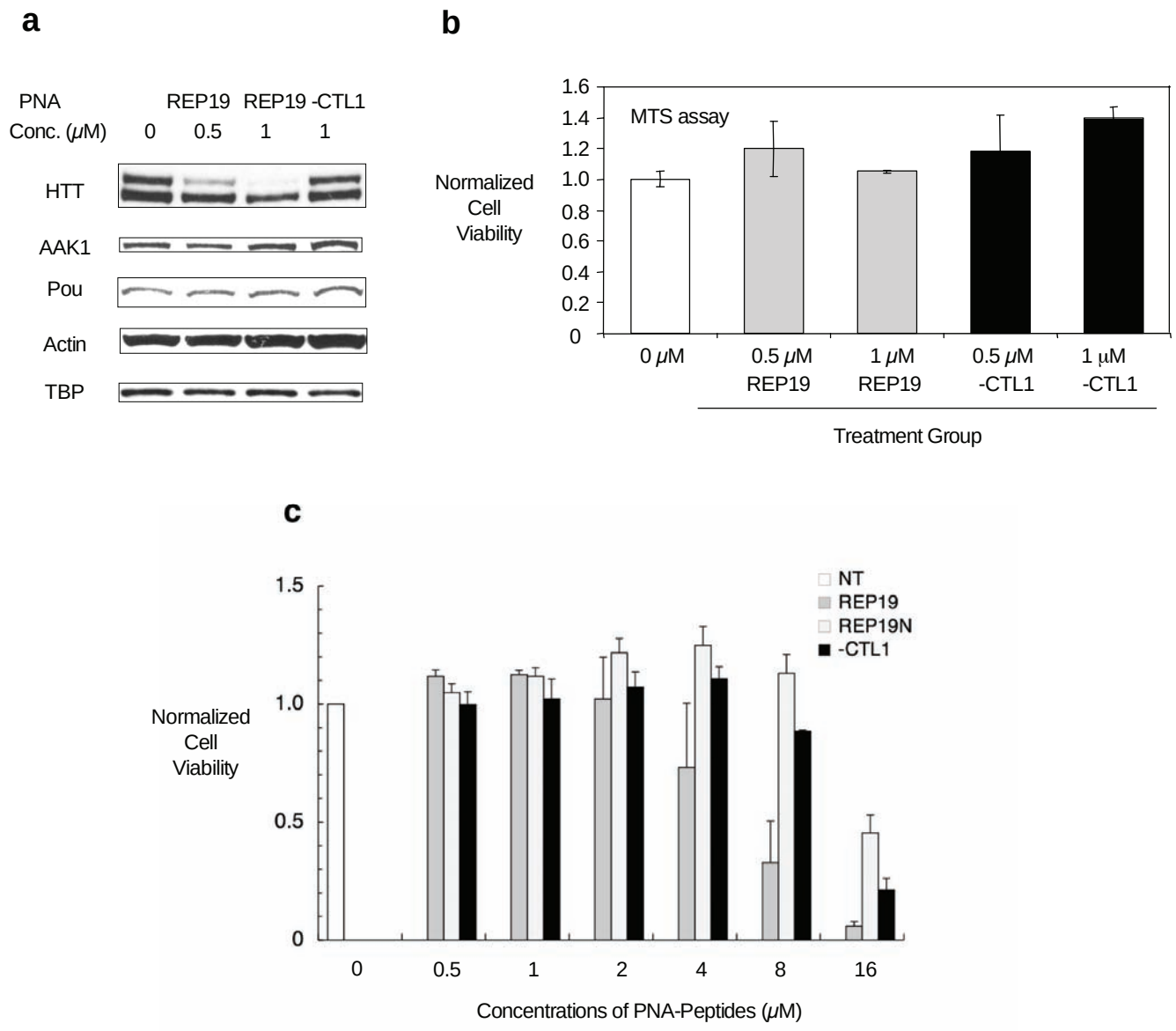

Supplementary Figure 4. Non-target effects of adding PNAs. (**a**) Effect of adding PNA REP19 on the expression of other proteins that contain CAG repeats within their mRNAs including AAK1, Pou, and TBP. Actin expression was monitored as an internal loading control. (**b**) Toxicity at PNA concentrations necessary for allele-specific inhibition of HTT expression (0.5 or 1 μM). No treatment (white bar). Fibroblast GM04281 cells were treated with REP19 (gray bar) or -CTL1 (black bar). (**c**) Toxicity at a wider range of concentrations, addition of PNAs REP19, REP19N, and -CTL1 at 0.5 to 16 μM. No treatment (white bar). Fibroblast GM04281 cells were treated withREP19 (dark gray bar), REP19N (light gray bar), and negative control -CTL1 (black bar). For (**b**) and (**c**), cell viability was evaluated using MTS assay (Promega). Error bars indicate s.d.; n=3 (b), n=4 (c).

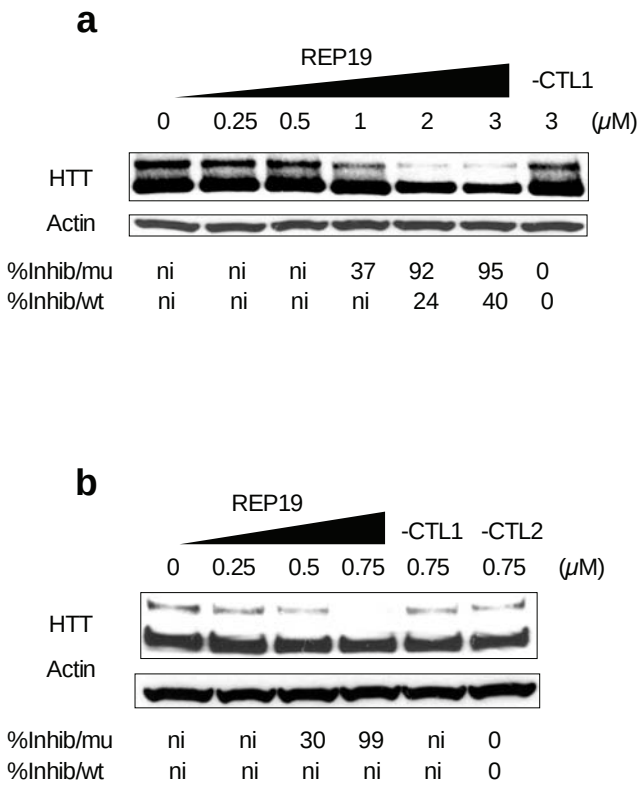

Supplementary Figure 5. **Inhibition of MSN/glial cell mixture by PNA REP19.** Medium striatal spiny neurons (MSN) and supporting glial cells were obtained from YAC128 mice and cultured as described in Materials and Methods. HTT protein levels were analyzed by western analysis. The top HTT band is human HTT and the bottom is murine HTT. PNAs REP19, –CTL1, or -CTL2 were added at the indicated concentrations. The amount of MSN relative to glial cells was estimated using light microscopy. (**a**) Effect of PNAs on MSN/glial cell mixture. Because glial cells make up approximately half of the cells in culture, data should not be taken as a direct indication of the level of inhibition of HTT in MSN cells. (**b**) Effect of PNAs on cells harvested with cell dissociation solution (Sigma). This dissociation protocol enriches MSN relative to glial cells (MSN:glials = 2:1) and offers a better indication of inhibition in MSN. Note that the apparent potency of inhibition increases with the percentage of striatal cells.

Nature Biotechnology: doi: 10.1038/nbt.1539

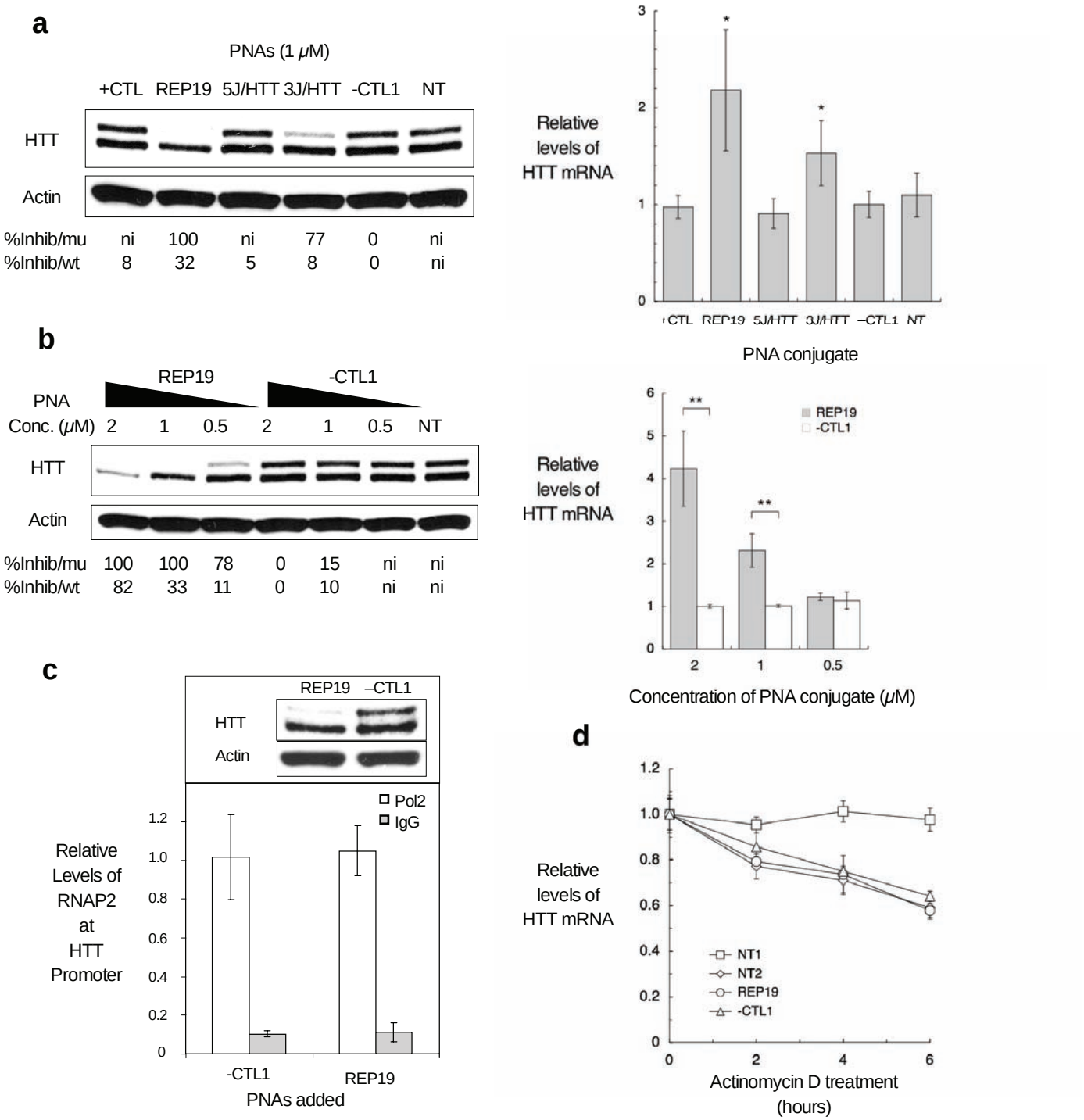

Supplementary Figure 6. Anti-HTT PNAs do not reduce HTT mRNA levels. (**a**) Western analysis and qPCR showing effect on levels of HTT mRNA of adding PNA-peptide conjugates at 1 μM, a concentration that achieves allele-selective inhibition. Measurements used GM04281 fibroblast cells. *p < 0.05 as compared to mismatch PNA peptide -CTL1. Error bars indicate s.d., n=4. (**b**) Western analysis and qPCR showing effect of adding REP19 at varied concentrations on expression of HTT mRNA. ** p < 0.01 as compared to mismatch PNA-peptide –CTL1; Error bars indicate s.d.; n=3. (**c)** Chromatin immunoprecipitation of RNAP2 on the HTT gene after addition of 1 μM of REP19 or mismatch-containing PNA –CTL1 shows no reduction of polymerase recruitment. Inset shows selective knockdown of mutant HTT by REP19 by western blot. Immunoprecipitation by a mouse IgG was included for comparison. **(d)** Effect of adding actinomycin D on levels of HTT mRNA after treatment with REP19. Four days after transfection ([REP19] or [-CTL1]=2 μM), each cell except for NT1 (no treatment sample 1) was treated with actinomycin D (5 μg/mL) for the indicated time (0, 2, 4, or 6 h). HTT mRNA level at each time point was determined by qPCR. GAPDH mRNA level was used for normalization. NT1: Not treated with PNA and not treated with actinomycin D. NT2: Treated with actinomycin D, but not treated with PNA.

a

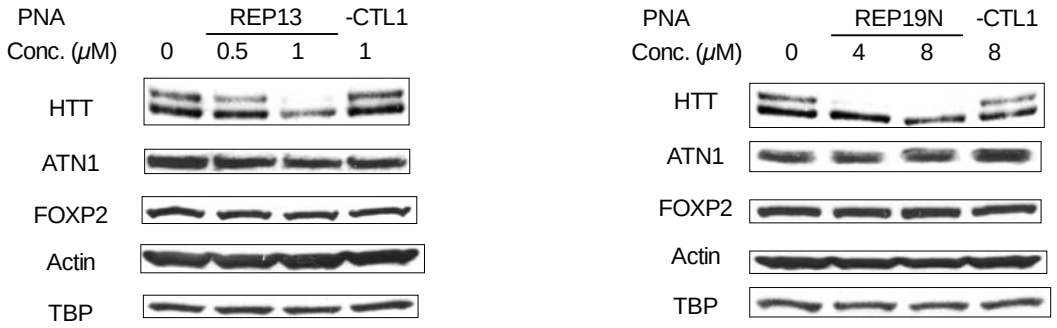

b

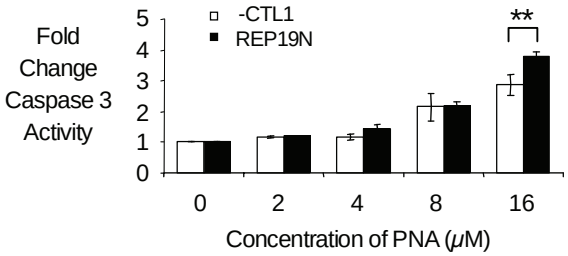

Supplementary Figure 7. Additional data on conjugates REP13 and REP19N. (**a**) Effect of adding REP13 or REP19N on expression of other proteins with mRNAs that contain CAG repeats. (**b**) Effect of adding REP19N on cell toxicity measured by monitoring levels of caspase 3. Caspase-3 activity was measured by hydrolysis of Ac-DEVD-pNA. $^{**}p < 0.01$, $n = 3$.

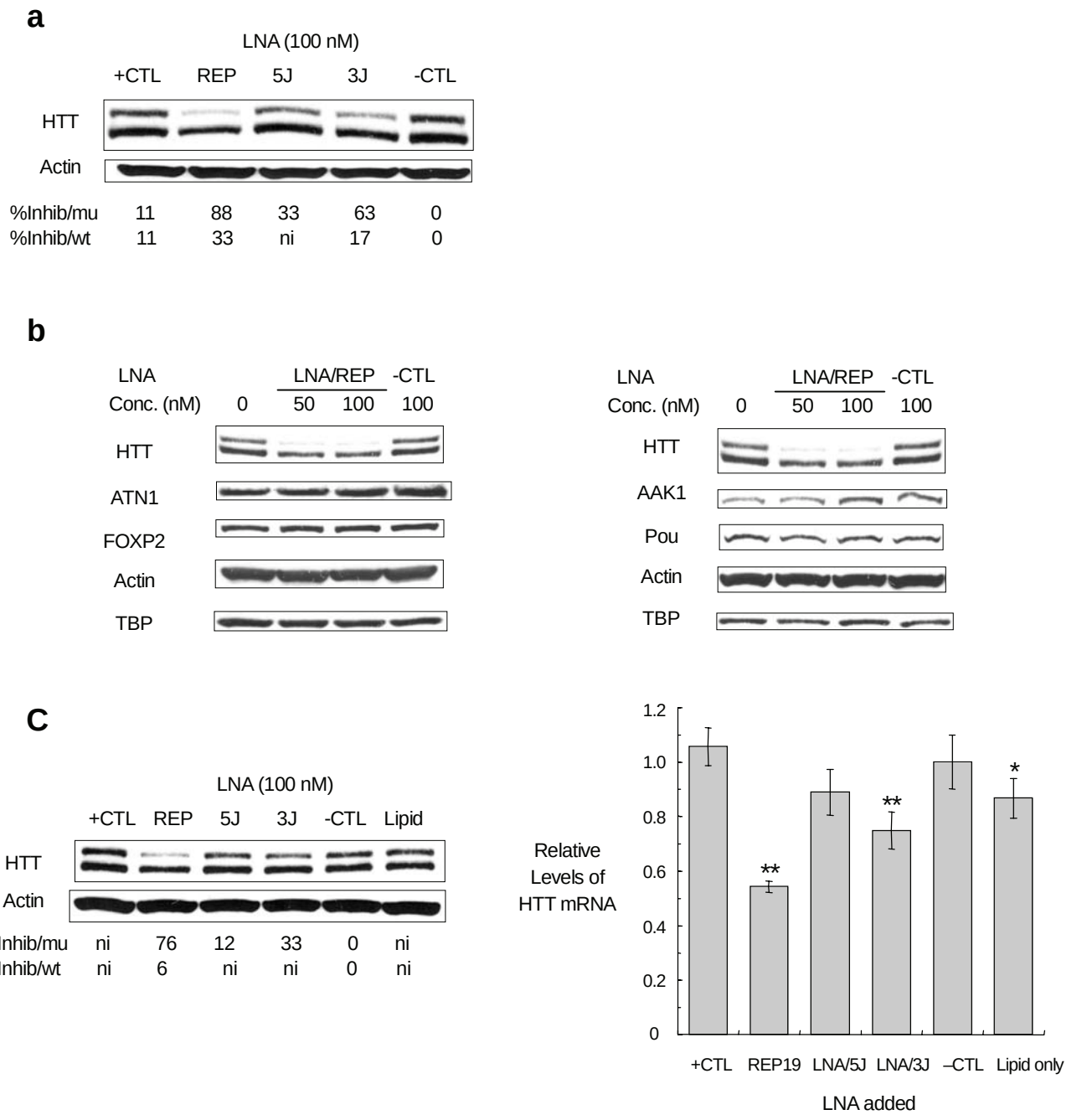

Supplementary Figure 8. Additional data on the effects of LNAs. (**a**) Effect on HTT expression of adding 100 nM LNAs. (**b**) Western analysis showing effect of adding LNA/REP on the expression of other proteins containing CAG repeats. (**c**) Western analysis and qPCR showing effect on HTT expression upon adding LNAs at 100 nM. ** $p < 0.01$, * $p < 0.05$ as compared to mismatch LNA (–CTL); Error bars indicate s.d.; n=6.

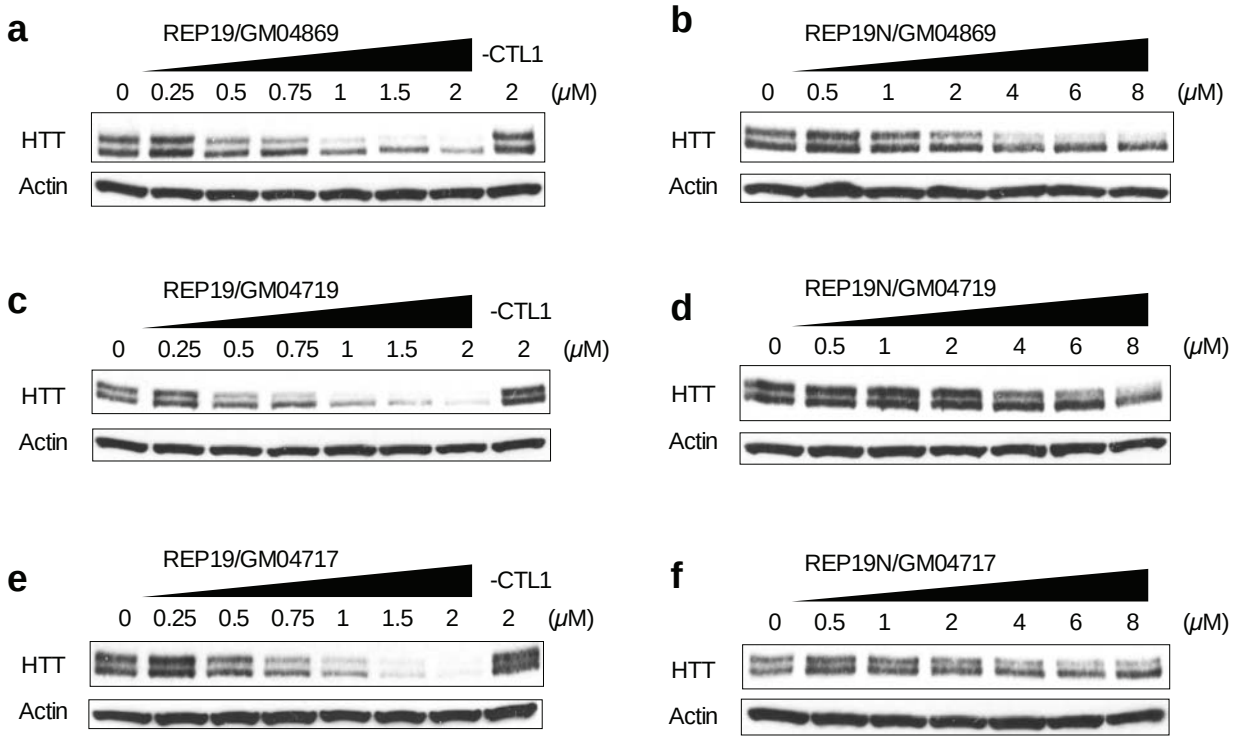

Supplementary Figure 9. Selectivity is affected by the number of repeats: Western analysis. Typical western gels underlying the graphical data in Figure 3. (**a**) Effect on HTT expression of adding REP19 to GM04869 cells. (**b**) Effect on HTT expression of adding REP19N to GM04869 cells. (**c**) Effect on HTT expression of adding REP19 to GM04719 cells. (**d**) Effect on HTT expression of adding REP19N to GM04719 cells. (**e**) Effect on HTT expression of adding REP19 to GM04717 cells. (**f**) Effect on HTT expression of adding REP19N to GM04717 cells.

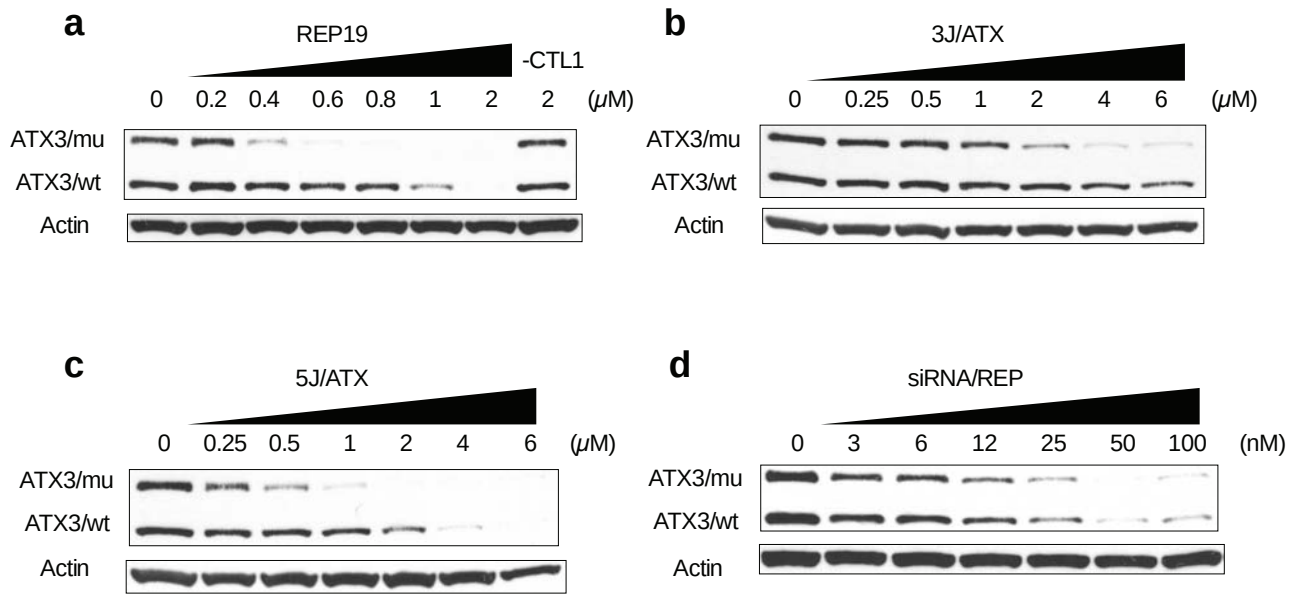

Supplementary Figure 10. Potent and selective inhibition of mutant ataxin-3. Typical western gels underlying the graphical data in Figure 4. All data show analysis of ataxin-3 expression in GM06151 fibroblast cells. **(a)** Inhibition of ataxin-3 expression by PNA conjugate REP19. (**b**) Inhibition of ataxin-3 expression by PNA conjugate 3J/ATX. (**c**) Inhibition of ataxin-3 expression by PNA conjugate 5J/ATX. (**d**) Inhibition of ataxin-3 expression by siRNA/REP.

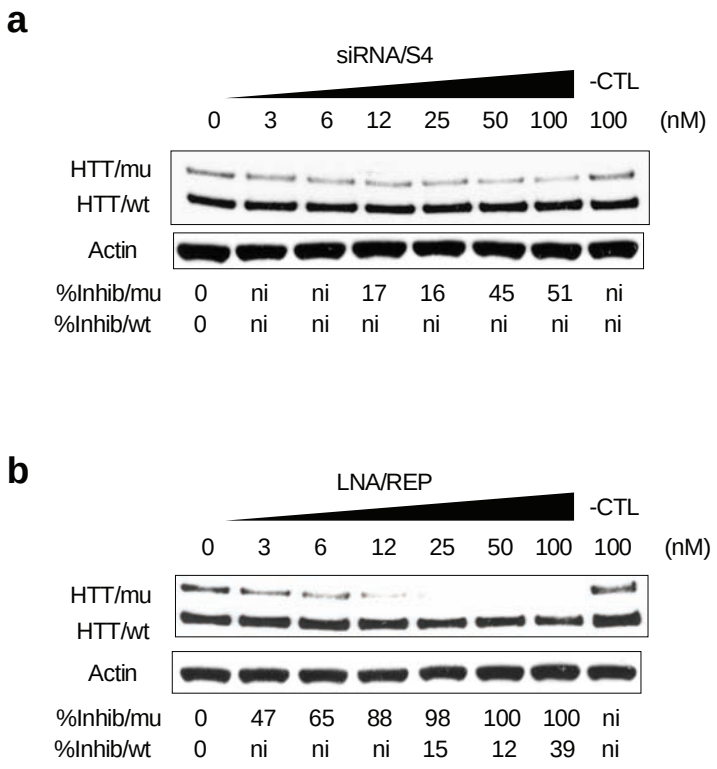

Supplementary Figure 11. Comparison of strategies targeting a deletion polymorphism to targeting CAG repeats. Effects on expression of HTT in GM09197 fibroblast cells (mutant allele with 151 CAG repeats/ wild-type allele with 21 CAG repeats). (**a**) Inhibition of HTT expression by siRNA S4 targeting a deletion polymorphism (Δ2642). (**b**) Inhibition of HTT expression by LNA/REP.

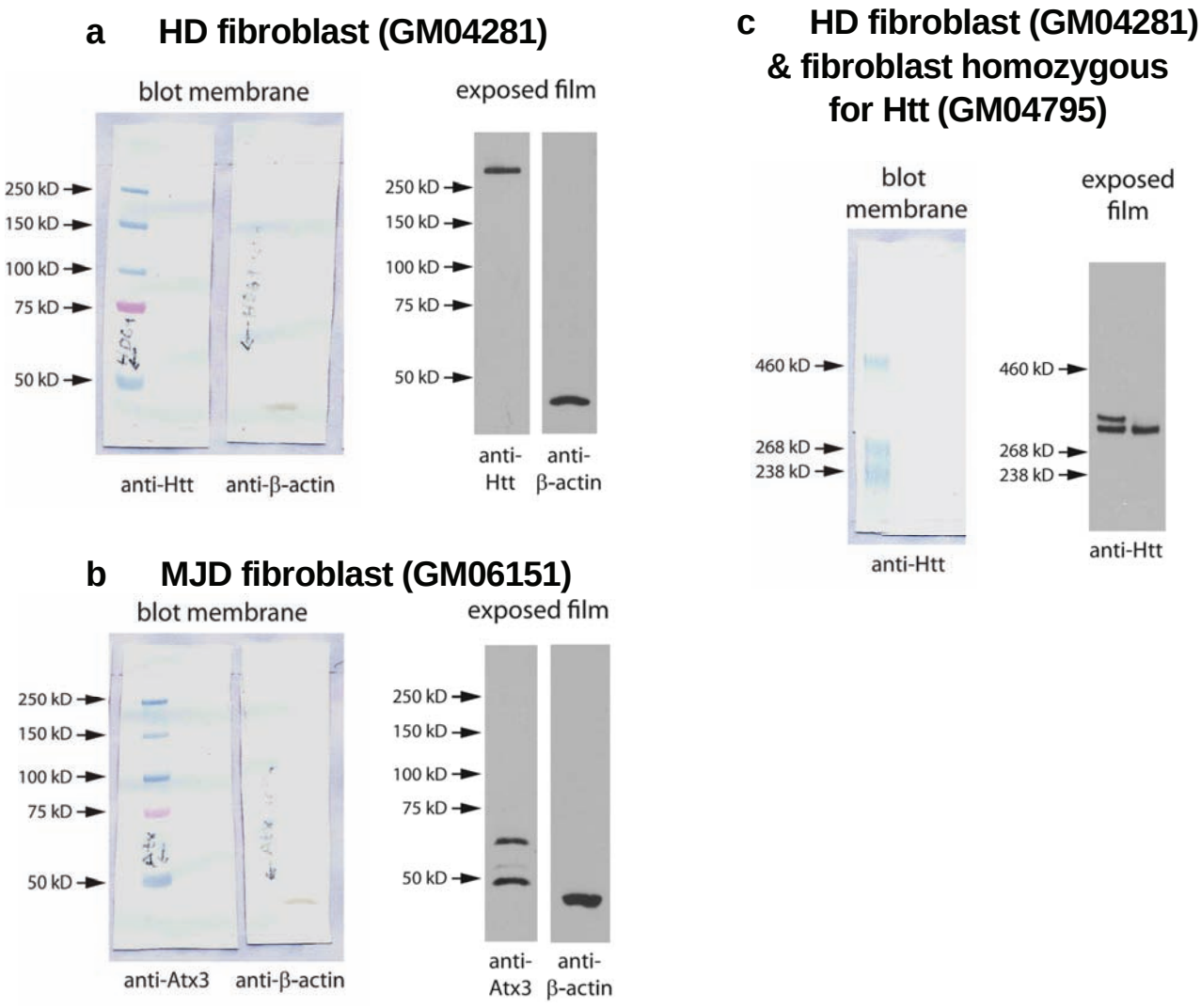

Supplementary Figure 12. Huntingtin and Ataxin-3 proteins are specifically detected by commercial antibodies in western blot assays. (**a**) A single, specific band appears after western blot detection of huntingtin (Htt) protein using the antibody MAB2166 (Chemicon). Total protein (20 μg) from Huntington Disease (HD) patient fibroblasts (GM04281) was resolved by SDS-PAGE on a precast 7.5% Tris-HCl Ready Gel (Bio-Rad) and resolved proteins were transferred onto nitrocellulose membranes, probed with antibodies against Htt or β-actin, and exposed to film (see Methods). A molecular weight standard (Precision Plus Dual Color Protein Standard, Bio-Rad) was resolved on the same gel and is shown after transfer to nitrocellulose (left panel). (**b**) Three specific bands appear after western blot detection of Ataxin-3 (Atx3) with the antibody MAB5360 (Chemicon), with the two major bands representing wild-type and mutant proteins. Total protein (20 μg) from Machado-Joseph Disease (MJD) patient fibroblasts (GM06151) was resolved by SDS-PAGE and Atx3 protein detected by western blot (see Methods). The Bio-Rad molecular weight standard used in panel A was resolved on the same gel and is shown after transfer to nitrocellulose (left panel). (**c**) Two specific bands corresponding to mutant and wild-type Htt protein are clearly observed by western blot detection after separation by SDS-PAGE on a 5% Tris-acetate gel (see Methods). Total protein (20 μg) from Huntington Disease (HD) patient fibroblasts (GM04281) (right panel, left lane) or fibroblasts homozygous for HTT (right panel, right lane) was resolved by SDS-PAGE and Htt protein detected by western blot as described in the Methods section. HiMark Pre-Stained High Molecular Weight Protein Standard (Novagen) was resolved on the same gel and is shown after transfer to nitrocellulose (left panel).

Figure 1c

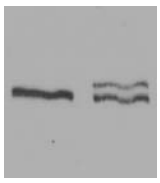

Figure 1d

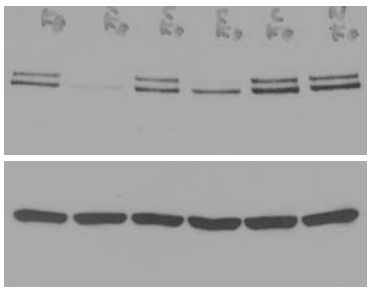

Figure 1g

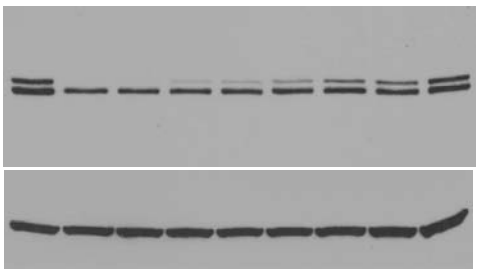

Figure 1h

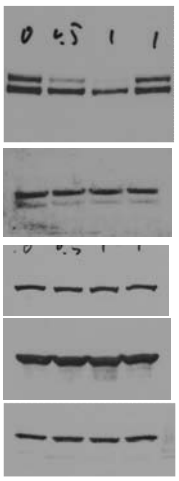

Figure 3a

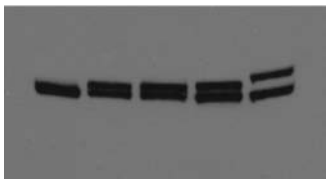

Supplementary Fig. 2a

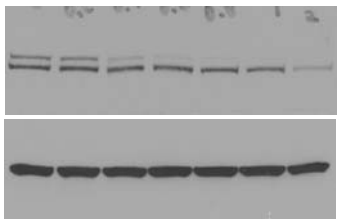

Supplementary Fig. 2b

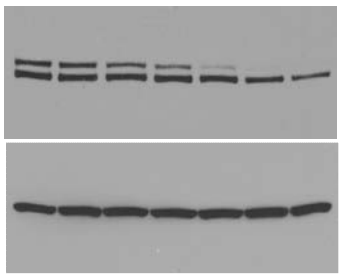

Supplementary Fig. 2c

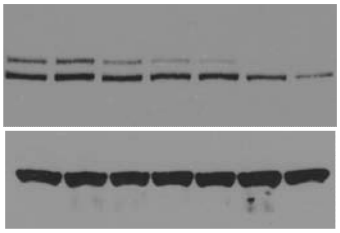

Supplementary Fig. 2d

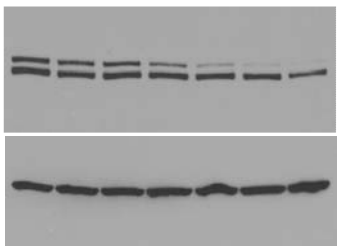

Supplementary Fig. 2e

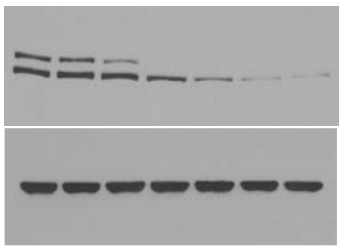

Supplementary Fig. 2f

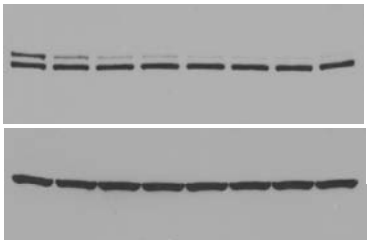

Supplementary Fig. 2g

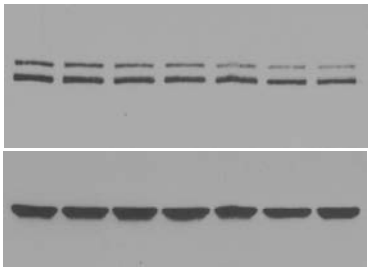

Supplementary Fig. 2h

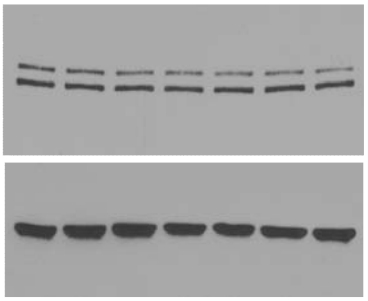

Supplementary Fig. 2i

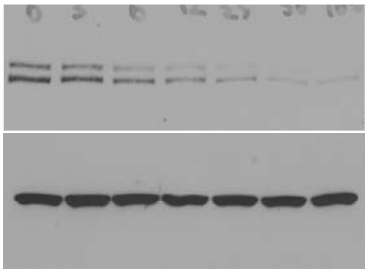

Supplementary Fig. 2j

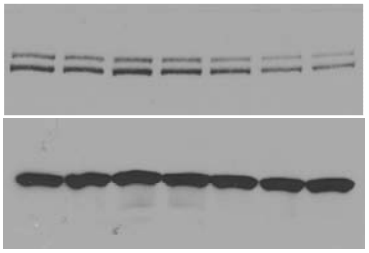

Supplementary Fig. 3b

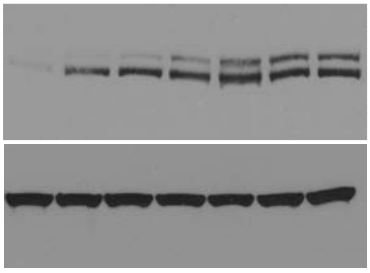

Supplementary Fig. 4a

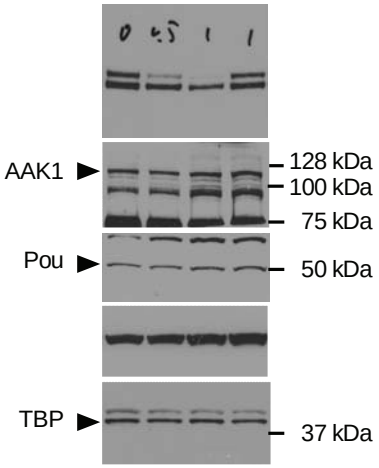

Nature Biotechnology: doi: 10.1038/nbt.1539

Supplementary Fig. 5a

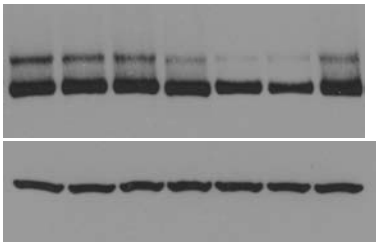

Supplementary Fig. 5b

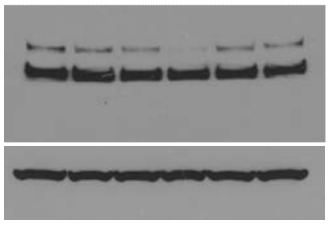

Supplementary Fig. 6a

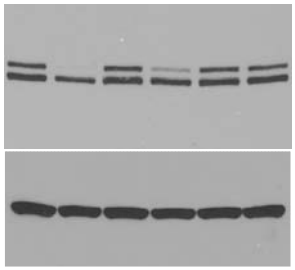

Supplementary Fig. 6b

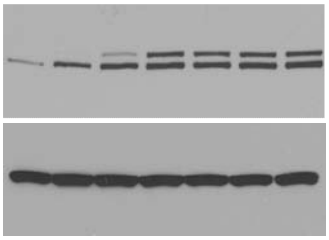

Supplementary Fig. 6c

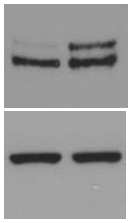

Supplementary Fig. 7a(left)

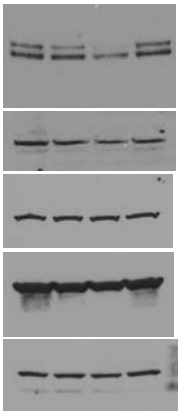

Supplementary Fig. 7a(right)

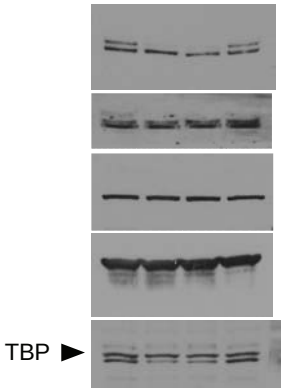

Supplementary Fig. 8a

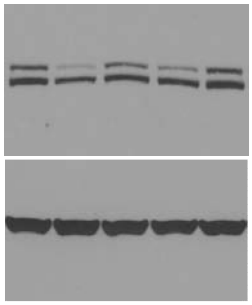

Supplementary Fig. 8b(left)

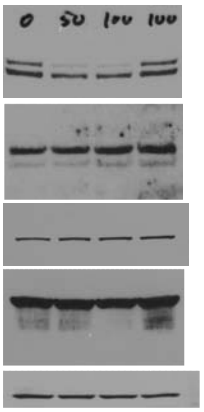

Supplementary Fig. 8b(right)

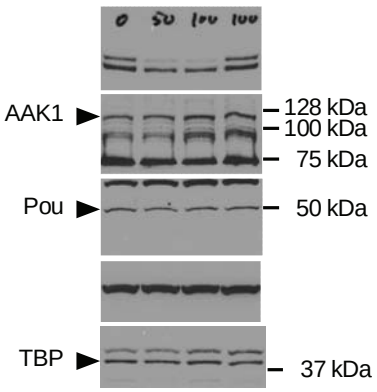

Supplementary Fig. 8c

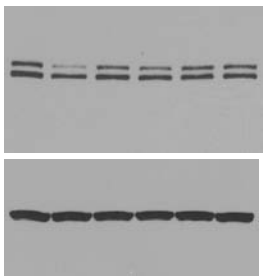

Supplementary Fig. 9a

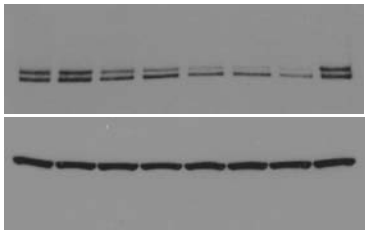

Supplementary Fig. 9b

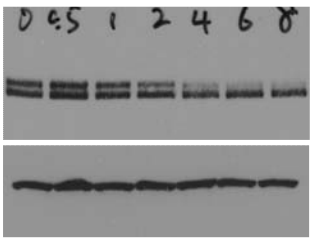

Supplementary Fig. 9c

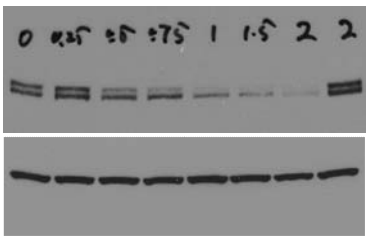

Supplementary Fig. 9d

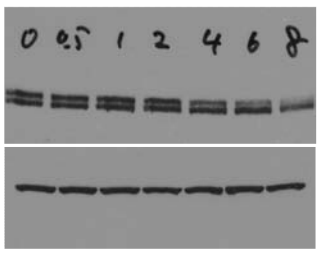

Supplementary Fig. 9e

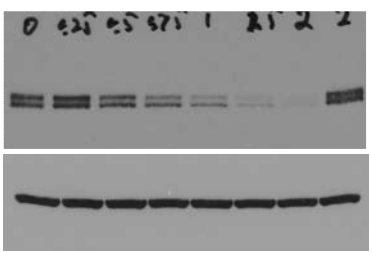

Supplementary Fig. 9f

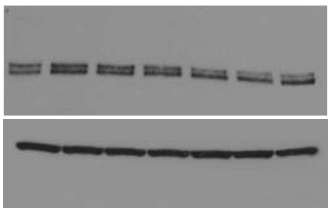

Supplementary Fig. 10a

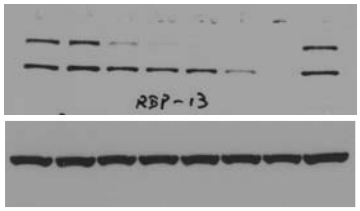

Supplementary Fig. 10b

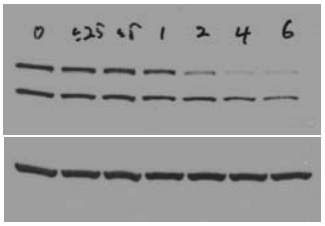

Supplementary Fig. 10c

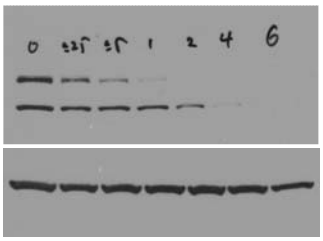

Supplementary Fig. 10d

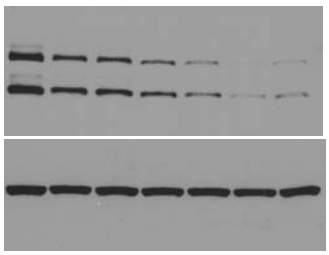

Supplementary Fig. 11a

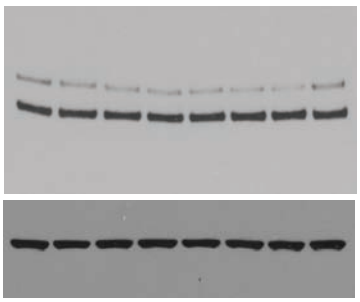

Supplementary Fig. 11b

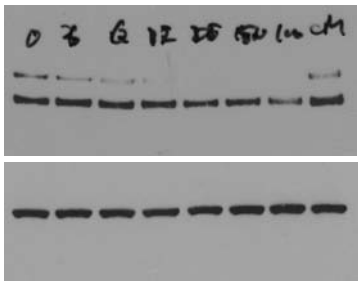

Supplementary Figure 13. Full scans of western blot data.